EFOP-3.6.1-16-2016-00018

Improving the role of research + development + innovation in the higher education through institutional developments assisting intelligent specialization in Sopron and Szombathely

Innovative processing technologies, applications of energy engineering and implementation of wide range techniques for microstructure investigation

Workshop on Innovative Materials Processing, Applications in Energy Engineering and System Control

ISBN 978-963-489-124-6

Szombathely, 2019

Workshop on Innovative Materials Processing, Applications in Energy Engineering and System Control
Chairpersons: Dr. Jurij SIDOR and Dr. László KOLLÁR
Date: February 22, 2019

Venue: Eötvös Loránd University, Faculty of Informatics, Savaria Institute of Technology, Károlyi Gáspár tér 4, 9700 Szombathely, Hungary
Room #: B209

Workshop is supported by EFOP-3.6.1-16-2016-00018 project: 'Improving the role of research + development + innovation in the higher education through institutional developments assisting intelligent specialization in Sopron and Szombathely'

Program

8.55-9.00 Jurij Sidor: ***Introduction***

9.00-9.15 Luis Rubio Rodriguez
Automated Control of Machining Processes
Eötvös Loránd University, Faculty of Informatics, Savaria Institute of Technology, Szombathely, Hungary.

9.15-9.30 Yiqing Meng and László E. Kollár
Active vibration absorber for aeolian vibration control on suspended cables
Eötvös Loránd University, Faculty of Informatics, Savaria Institute of Technology, Szombathely, Hungary.

9.30-9.45 László E. Kollár
Aerodynamic Performance Degradation of Wind Turbine Blades due to Ice Accretion
Eötvös Loránd University, Faculty of Informatics, Savaria Institute of Technology, Szombathely, Hungary.

9.45-10.00 Kristóf Lajber
Development of an intelligent vehicle control system
Eötvös Loránd University, Faculty of Informatics, Savaria Institute of Technology, Szombathely, Hungary.

10.00-10.15 József Szőlősi
Designing of beam welding technologies for carbon steel structures
Eötvös Loránd University, Faculty of Informatics, Savaria Institute of Technology, Szombathely, Hungary.

10.15-10.30 Tibor Borbély and Jurij J. Sidor
Rolling mill design challenges
Eötvös Loránd University, Faculty of Informatics, Savaria Institute of Technology, Szombathely, Hungary.

10.30-10.45 Dániel Fenyvesi and Jurij J. Sidor
Finite Element modelling of deformation flow in symmetric and asymmetric rolling processes
Eötvös Loránd University, Faculty of Informatics, Savaria Institute of Technology, Szombathely, Hungary.

10.45-11.00 Gyula Pál and Jurij J. Sidor
Comparison of microstructure evolution after symmetric and asymmetric rolling
Eötvös Loránd University, Faculty of Informatics, Savaria Institute of Technology, Szombathely, Hungary.

11.00-11.15 Jurij J. Sidor
Application of polycrystal models to simulation of texture evolution in thermo-mechanical processing of metals
Eötvös Loránd University, Faculty of Informatics, Savaria Institute of Technology, Szombathely, Hungary.

11.15 Closing Remarks

Each talk includes 12 min of presentation and 3 min of discussion

Abstracts

Automated Control of Machining Processes

Luis Rubio Rodriguez
Eötvös Loránd University, Faculty of Informatics, Savaria Institute of Technology, Szombathely, Hungary
e-mail: l.rubio.r@gmail.com

Abstract. This work outlines main characteristics of computer controlled machining processes. First, an overview of the control system architecture is given. The developed control system consists of three parts, namely, servo, process and supervisory controllers.
Servo controller follows a predefined trajectory or contouring minimizing errors. Some control algorithms are displayed and compared to this aim. The control algorithms are based on traditional industrial PID and more sophisticated sliding mode controllers.
Process controller can be split, at the same time, in three parts, force controller, vibrations detection and suppression and, tool monitorization for wear estimation. An adaptive control force scheme is addressed. Some algorithms to detect and suppress chatter are also pointed out. Furthermore, a block diagram about tool wear monitorization is presented.
Finally, supervisory control loop is provided. It is based on some external inputs such as process constraints, strategy to follow and required performance indexes. Supervisory control outputs suggestions about tool and process selection, programmed feed rate and speeds, required input commands to the control system, control strategies which have to be performed, and how to manage time-delays in the control system.

Active vibration absorber for aeolian vibration control on suspended cables

Yiqing Meng and László E. Kollár
Eötvös Loránd University, Faculty of Informatics, Savaria Institute of Technology, Szombathely, Hungary
e-mail: my@inf.elte.hu and kl@inf.elte.hu

Abstract. The vibration problems in power transmission conductors and cable-supported bridges, significantly affects the strength and durability of cables and may lead to failure of other elements of the structure. Special attention should be paid to the cable oscillation due to wind actions characterized by high frequency and small amplitude, which is called aeolian vibration. Many conventional anti-vibration techniques have been developed and are in current use in the field, such as Stockbridge damper, impact damper, friction damper etc., but there are severe limitations regarding to their implementation and control reliability. Active vibration control techniques have been successfully used in many industrial applications to attenuate the vibration amplitude due to various disturbances; however, only a small number of results can be found in the published literature concerning the problem of active control of cable vibration. This study presents the design of an active vibration absorber system, employing a conventional vibration absorber with actuator and control algorithm, for controlling the vibration of such suspended cables as the transmission line conductor or the cable of cable-stayed bridges. A number of numerical simulations were carried out in the SIMULINK environment using two different control algorithms. One of them is based on PID controller, and the other one estimates cable vibration frequency to determine the dynamic performance of the controller. The simulation results show that both control algorithms lead to a strikingly faster vibration amplitude attenuation than a passive vibration absorber.

Aerodynamic Performance Degradation of Wind Turbine Blades due to Ice Accretion

László E. Kollár
Eötvös Loránd University, Faculty of Informatics, Savaria Institute of Technology, Szombathely, Hungary
e-mail: kl@inf.elte.hu

Abstract. Ice accretion on a 2D section of wind turbine blades is simulated with the specific aim to estimate the aerodynamic performance degradation of the iced blade. The ice accretion model simulates the air flow around the blade, determines the trajectories of water droplets, and calculates the ratio of droplets that freeze on the blade surface. The air flow is then simulated around the iced blade surface, and simulation results provide the lift coefficient and drag coefficient. The ratio of these aerodynamic parameters is compared with the same ratio obtained for the bare blade. This process is repeated for blade shapes with varying camber line, which provides the severity of aerodynamic performance degradation for different blade shapes. The study reveals that the reduction in the lift-to-drag ratio increases as the blade shape approaches the symmetric shape. The consideration of these results in the design process contributes to finding blade shapes that can be used under some icing conditions.

Development of an intelligent vehicle control system

Kristóf Lajber
Eötvös Loránd University, Faculty of Informatics, Savaria Institute of Technology, Szombathely, Hungary
e-mail: lk@inf.elte.hu

Abstract. The SZIe-Kart team has needed an easily expandable, robust, high performance control system for the Go-Kart Go-Bosch competition, which is capable to withstand the rough automotive environment. The system had to be flexible enough to solve the complex process control problems. Therefore, I designed a modular system with microcontrollers, where the controllers are communicated trough CAN bus. I changed the previously used Arduino based Atmel AVR controllers with Texas Instruments (TI) MCU's. The main aspects of the selection was the better documentation, the built in CAN module, and the TI's own Boosterpack system. The modular design and the use of CAN bus allows to test the modules severally.
For the software development I choose the Energia environment, which allows using the object-oriented C++ language. The benefits of this environment, and language that it's a user friendly quickly learnable method. The high level programming was supported by the TI's Driverlib, what creates a bridge between the object oriented programing and the hardware which makes the software development faster, easier. To implement the function defined by the Bosch, they provided us different sensors. These sensors used CAN bus to provide us with the necessary information. To realize the Driver Assistance (DA) functions we had to add our own sensors too. I had to take these parameter into consideration at the design process. To realize the DA functions in the go-kart I had to design the necessary actuators such as electric gas for the petrol engine, electric brake system, and a power steering. The strict safety regulations made designing these more challenging.
These days making an efficient Human Machine Interface is a high priority task, therefore my goal was to develop a Glass Cockpit (like the airplanes) with touch LCD screens as primary

input, and output device. The competition required a wireless telemetry function. I designed the telemetry primary to send state properties to a distant observation point.

Designing of beam welding technologies for carbon steel structures

Szőlősi József
Eötvös Loránd University, Faculty of Informatics, Savaria Institute of Technology, Szombathely, Hungary
e-mail: szolosjo@googlemail.com

Abstract. This contribution describes the current production process of welding, as the research of technology can only stem from the awareness of the technological features and possibly of what waste could be eliminated in the original situation. The work is focusing on review the current research fields related to the topics of high-pressure welding, classical technology planning process and the conditions of weldability. Particularly, the production technology conditions of crack-free structures, with a special focus on defining the necessary pre-heating temperature, are discussed in detail. For the investigation I used the test results of the laser-hybrid welding. These tests were performed with the professional support of the Crown International Kft - Cloos representative.

Rolling Mill Design Challenges

Borbély Tibor and Jurij J. Sidor
Eötvös Loránd University, Faculty of Informatics, Savaria Institute of Technology, Szombathely, Hungary
e-mail: bt@inf.elte.hu and js@inf.elte.hu

Abstract. In forming technologies, the laboratory experimental equipment is more compact as compared to the industrial counterparts. The laboratory facilities are usually produced in smaller series, however, they are designed for a particular purpose and manufactured by specialized companies to meet the needs of a particular research site. Conventional rolling mills are generally suitable only for symmetrical rolling where the circumferential velocity of both cylinders is identical. In the case of asymmetric rolling, the rolls are driven by separate motors to ensure different circumferential velocities.
Current contribution discusses numerous issues related to the design of a rolling mill suitable for both conventional and asymmetric rolling. In the present project planning, it was necessary to account for the main characteristics of conventional constructions, and in view of this, a specific strategy had to be developed, corresponding to a given purpose. Using a mill, which is suitable for asymmetric rolling, it is possible to introduce a large amount of shear deformation into the rolled material, which can be realized by conventional (symmetric) rolling only by employing the cylinders of significantly different roughness or by varying the friction conditions of the upper and lower roll surfaces.

Finite Element Modelling of Deformation Flow In Symmetric And Asymmetric Rolling Processes

Dániel Fenyvesi and Jurij J. Sidor
Eötvös Loránd University, Faculty of Informatics, Savaria Institute of Technology, Szombathely, Hungary
e-mail: fd@inf.elte.hu and js@inf.elte.hu

Abstract. Processing technology of metals involves cold rolling, which triggers plastic deformation in a material, subjected to thickness reduction. In the course of symmetric rolling, the compressive component of the three-dimensional deformation tensor is dominating over other ones, whereas, the asymmetric mode accounts for a substantial amount of shear deformation. Additionally, the asymmetric loading is partially caused by both the different friction conditions of the surfaces and the variety in angular velocities of cylinders. This contribution discusses the results of finite element simulation (FEM) of 6063 aluminium alloy subjected to symmetric and asymmetric loading. Ansys Mechanical APDL solver was employed for the FEM calculations. The simulations were performed for non-linear static case, where the roll is considered as a rigid body, whereas the angular velocities of the upper and lower rolls were different with the aim to introduce asymmetry. In this two-dimensional calculation, it was assumed that the material rolled does not suffer any widening. The hexagonal meshing was used, while it appeared that accurate simulation requires a high number of elements through thickness. Therefore, the number of elements across the thickness was varying between 10 and 12. Results of the FEM simulations are presented in a form of strain velocity gradients, strain and stress distributions across the thickness of rolled sheets.

Comparison of microstructure evolution after symmetric and asymmetric rolling

Gyula Pál and Jurij J. Sidor
Eötvös Loránd University, Faculty of Informatics, Savaria Institute of Technology, Szombathely, Hungary
e-mail: pg@inf.elte.hu and js@inf.elte.hu

Abstract. Common manufacturing process of the semi-finished aluminium products is rolling. The product of this process is widely used in automotive and aerospace industry due to the advantage what it offers such as good availability, high corrosion resistance, better strength-to-density ratio, as compared to unalloyed steel grades. Because of the elevating expectations of above-mentioned industries, it is important to perform evaluations related to reduction of the main drawbacks as the poor manufacturability and formability. The key parameters, which determine the formability, reveal a strong relationship with the crystallographic texture.
The texture formation in face-centered cubic materials like aluminium alloys is related to the evolution of several kinds of crystal defects in the dimension range from nm to mm. Presence of a pronounced texture leads to a strong anisotropy, because the deformation spreads in different ways among various crystals, and this limits the practical application of conventional manufacturing processes. This contribution focuses on a comparison between the microstructural changes developed during conventional/symmetrical and non-conventional/asymmetric cold rolling.
The comparison is based on texture examinations, which reveal that during conventional cold rolling a β-fibre texture tends to develop and disappears during the recrystallisation followed

by deformation. The annealing microstructure poses a characteristic texture comprising cube, Goss and P-components. These textures cause low normal anisotropy value in aluminium, which is considered to be undesirable from the point of view of deep drawability. In the case of asymmetric rolling the specimen is subjected to more severe shear deformation, which results in a shear-type texture. Consequently, microstructure evolved after annealing has more appropriate texture for further deep drawing.

Application of polycrystal models to simulation of texture evolution in thermo-mechanical processing of metals

Jurij J. Sidor
Eötvös Loránd University, Faculty of Informatics, Savaria Institute of Technology, Szombathely, Hungary.

Abstract. Industrially produced metals are usually polycrystalline aggregates with characteristic crystallographic textures. The key microstructural feature such as a grain size is strongly correlated to mechanical properties, however, the anisotropy of properties is mainly affected by means of texture evolved. The evolution of texture occurs over the entire thermo-mechanical processing and the control of this development occurs via tuning of manufacturing parameters. The degree of reduction, number of deformation steps, annealing temperature or heating/cooling rate have a strong impact on both microstructure and texture development. In this view, it is very important to control the key microstructural parameters during each production step and this is possible via linking the external macroscopic influences to the mesoscopic features. The numerical approaches are of great importance in resolving this issue. Current contribution focuses on the implementation of various polycrystal models in prediction of texture evolution in Al alloys during processing. Based on modelling approaches, it is discussed how technological parameters affect both texture evolution and related properties.

Short communications

Computer Numerical Control Machining

Luis Rubio

Savaria Institute of Technology
ELTE Eötvös Loránd University, Budapest, Hungary
lrr@inf.elte.hu

Abstract
Some aspects about machining control are reviewed in this paper. It is given a step ahead in the field of trajectory tracking proposing a super-twisting sliding mode control. Moreover, novel strategies for adaptive force control, chatter vibrations avoidances are included in a more sophisticated expert system.

Keywords: CNC Machining, Sliding Mode Position Control, Adaptive Force Control and Chatter Vibrations.

Introduction

This study pictures out the ground covered in advanced control systems in machining. Cutting forces need to be under prescribed upper limit in order to avoid tool fracture or breakage and excessive wear. Therefore, first, super-twisting sliding mode control tracks pre-defined desired trajectories in order to overcome the influences of disturbances and model uncertainties designed based on plant modelling. Secondly, a novel adaptive control scheme of forces outputs the tracking reference signal against sudden changes in machining parameters such as cutting conditions. Finally, an expert system incorporates the adaptive control of forces while avoids chatter vibrations in a multi-objective optimization for Pareto optimal cutting parameter sets. Moreover, strategies for chatter detection and control and a supervisory system are included.

Methodology

Figure 1 shows the control system architecture which is composed by three layers, servo control, process control and supervisory control. Servo controller manoeuvers axis and spindle drives. Process controllers fix constraints regarding upper forces to avoid wear, tool breakage and vibrations. Finally, supervisory control feedbacks products dimensions and surfaces to close the loop.

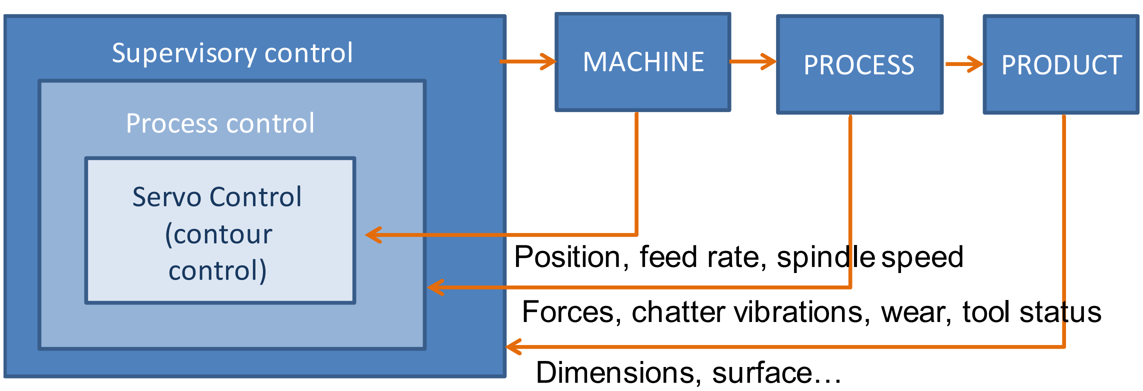

Fig. 1: Overview of the machining control process, servo, process and supervisory control.

Results

The following results were obtained:

a) Different control algorithms has been proposed and compared to track pre-defined positioning reference signal (figure 2) [1], comparisons can be seen on table 1;

b) novel adaptive control strategies have been implemented in order to established the cutting forces under prescribed upper limit (figure 3) [2];

c) Supervisory control general scheme;

d) Expert system implementation for Pareto optimal cutting parameters selection with multi-objective optimization [3] and chatter deteccion and avoidance;

a) Servo controller: comparison of different control schemes

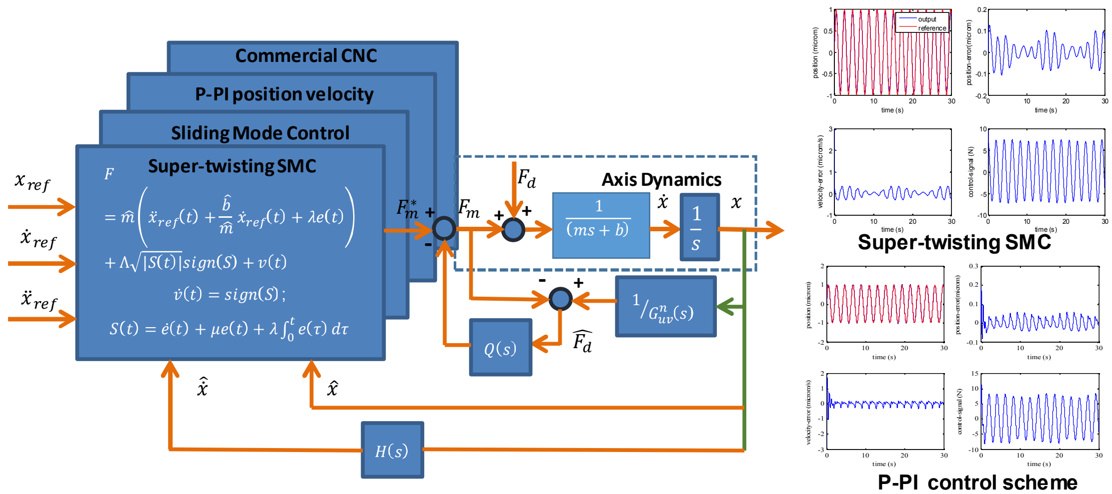

Fig. 2: Realization and outputs of different control algorithms for 1-axis servo drives.

	Position error		Velocity error	
	max	σ	max	σ
Aerotech without disturbances	0.1826	0.0178	1.9014	0.2096
Aerotech with disturbances	0.1895	0.0307	1.6910	0.2339
SMC without disturbances (fig. 6)	0.059	0.0186	3	0.0790
SMC with disturbances (fig. 7)	0.0604	0.0189	3	0.0855

Table 1: Numerical comparison of different control algorithms for 1-axis servo drives.

b) Process control: Novel approaches for adaptive control of forces

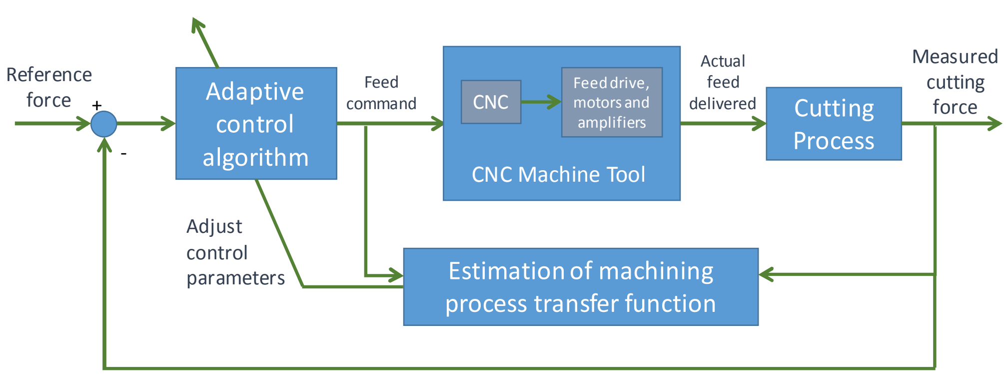

Fig. 3: Adaptive control algorithms for cutting forces. Realization in [2] and references therein;

c) Supervisory control general scheme

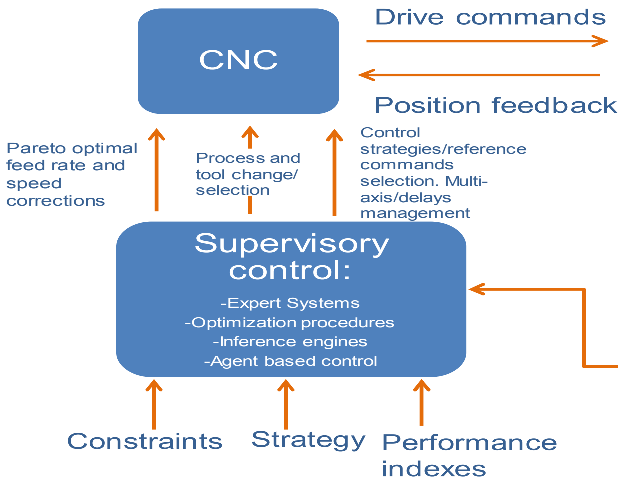

Fig. 4: Supervisory control scheme.

d) Expert system to select Pareto optimal cutting parameters (supervisory control) and chatter detection and avoidance (process control)

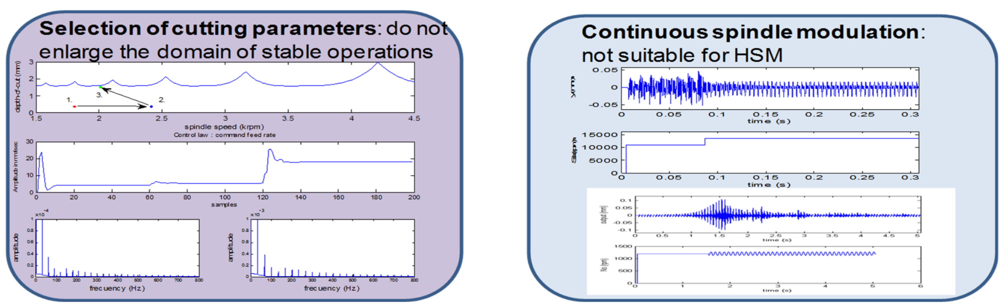

Fig. 5: Realization of an expert system and chatter detection and avoidance.

Acknowledgment

The research was published in the frame of the project "EFOP-3.6.1-16-2016-00018 – Improving the role of research + development + innovation in the higher education through institutional developments assisting intelligent specialization in Sopron and Szombathely".

References

[1] Rubio L., Ibeas A. and Luo X., "P-PI and super-twisting sliding mode control schemes comparison for high-precision CNC machines", 24th Iranian Conf. on El. Eng., 2016.

[2] Rubio L. et al., "Analysis of discrete time schemes for milling forces control under fractional order holds", Int. J. of Prec.Eng. and Manuf.14 (5), pp. 735-744, May 2013.

[3] Rubio, L. et al., *Model-Based Expert System to automatically adapt milling forces in Pareto optimal multi-objective working points*, Expert Systems with applications, 2013.

Active vibration absorber for aeolian vibration control on suspended cables

Yiqing Meng[1], Laszlo E. Kollar

Savaria Institute of Technology
ELTE Eötvös Loránd University, Budapest, Hungary

my@inf.elte.hu, kl@inf.elte.hu

Abstract
The vibration problems in the cable-supported bridges, significantly affects the strength and durability of cables and may lead to failure of other elements of the structure. Special attention should be paid to the cable oscillation due to wind actions characterized by high frequency and small amplitude, which is called aeolian vibration. Many conventional anti-vibration techniques have been developed and are in current use in the field, such as Stockbridge damper, impact damper, friction damper etc., but there are severe limitations regarding to their implementation and control reliability. Active vibration control techniques have been successfully used in many industrial applications to attenuate the vibration amplitude due to various disturbances; however, only a small number of results can be found in the published literature concerning the problem of active control of cable vibration. This study presents the design of an active vibration absorber system, employing a conventional vibration absorber with actuator and control algorithm, for controlling the vibration of such suspended cables as the cable of cable-stayed bridges. A number of numerical simulations were carried out in the SIMULINK environment using two different control algorithms. One of them is based on PID controller, and the other one estimates cable vibration frequency to determine the dynamic performance of the controller. The simulation results show that both control algorithms lead to a strikingly faster vibration amplitude attenuation than a passive vibration absorber.

Keywords: active vibration control, cable-supported bridge, PID controller

Introduction

Over last decades the long span bridge has been developed and used in many countries [1]. As an essential component of structure of the bridge suspended cables play an important role in the dynamic behaviour of cable-supported bridges. However, there is a well-marked problem improving the safety of the cable-supported bridges due to the cables are highly vulnerable to the wind induced vibration; especially for high-speed vortex shedding excitation. The vortex shedding often gives rise to the varying wind forces around cable that are caused the aeolian vibration problem. The frequency of vibration is usually in the range of 4Hz to 100Hz with a wind speed of 1-10m/s [2]. Aeolian vibration inflicts damage on the cable within period of time and this may cause more serious accidents and considerable economic loss. A number of technologies have been invented and developed so as to manage the problem, such as traditional viscous dampers and mechanical spacers[3]. According to several papers in the literature[4, 5], the calibration and reliabilities are considered to be the major limitations of these techniques due to calibration procedures being relatively complicated and the fact that the parameters obtained in the laboratory calibration system may not be valid for the suspended cable in real bridges. In this study active vibration control methods are used to control suspended cable of the bridge. State space theory will be used in order to describe the dynamic motion of the system. The control algorithm and simulation are carried out by using SIMULINK.

[1] Corresponding author

Dynamic model

The fundamental of aeolian vibration control by using active controller can be considered as a two-degrees-of-freedom (2DOF) system shown in Fig.1, where the cable mass and the controller mass are represented by m1 and m2, respectively. The control objective of this system is to generate control force between m1 and m2 to keep the displacement of m1 in a safe range when the wind force imposed into the cable (m1).

From the model shown in Fig.1, the differential equation of the system (1) is obtained by using the Newton's law

$$M\ddot{X} + C\dot{X} + KX = Q \qquad (1)$$

where

$$M = \begin{bmatrix} m_1 & 0 \\ 0 & m_2 \end{bmatrix};\ C = \begin{bmatrix} c_1 + c_2 & -c_2 \\ -c_2 & c_2 \end{bmatrix};\ K = \begin{bmatrix} k_1 + k_2 & -k_2 \\ -k_2 & k_2 \end{bmatrix};\ X = \begin{bmatrix} x_1 \\ x_2 \end{bmatrix} Q = \begin{bmatrix} F - f_c \\ f_c \end{bmatrix}$$

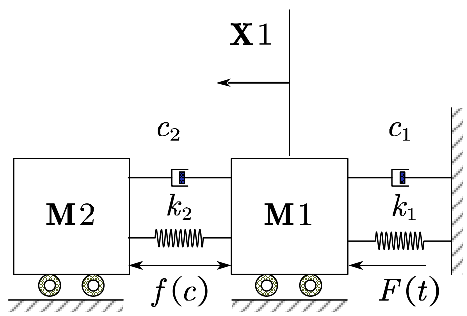

Fig.1 Dynamic model of cable and controller system

The dynamic cable vibration model can be expressed as a state-space model of the form:

$$\dot{\overline{X}} = A\overline{X} + BU \qquad (2)$$

$$Y = E\overline{X} \qquad (3)$$

where

$$\dot{\overline{X}} = \begin{bmatrix} \dot{x}_1 \\ \ddot{x}_1 \\ \dot{x}_2 \\ \ddot{x}_2 \end{bmatrix}; A = \begin{bmatrix} 0 & 1 & 0 & 0 \\ -\frac{k_1 + k_2}{m_1} & -\frac{c_1 + c_2}{m_1} & \frac{k_2}{m_2} & \frac{c_2}{m_1} \\ 0 & 0 & 0 & 1 \\ \frac{k_2}{m_2} & \frac{c_2}{m_2} & -\frac{k_2}{m_2} & -\frac{c_2}{m_2} \end{bmatrix}; \overline{X} = \begin{bmatrix} x_1 \\ \dot{x}_1 \\ x_2 \\ \dot{x}_2 \end{bmatrix} \qquad B = \begin{bmatrix} 0 & 0 \\ \frac{1}{m_1} & -\frac{1}{m_1} \\ 0 & 0 \\ 0 & \frac{1}{m_2} \end{bmatrix};$$

$$U = \begin{bmatrix} F \\ f_c \end{bmatrix}; E = \begin{bmatrix} 1 & 0 & 0 & 0 \end{bmatrix}$$

It is worth noting that the k1, k2, c1, c2 represent the spring constant of the cable, spring constant of the vibration controller, the damping ratio of the cable and damping ratio of vibration controller, respectively. In addition, *F* is the wind induce force and *fc* is the control force which is delivered by the control system.

Controller

The first control methodology is based on use of conventional PID and was implemented through the vibration absorber system which is located between the cable and mass (m2). The PID controller is by far the most popular and robust algorithm of solving practical control problem[6, 7]. Fig.2 shows that the PID controller was implemented to reduce the displacement of x1 by using SIMULINK software. After obtaining the optimum PID parameters and the mechanical absorber, performance of close loop PID based vibration control system needs to be verified. By simulation, the comparison results between using mechanical passive controller and PID controller are shown in Fig.3: the black line, yellow line and red line are the response of the free vibration system(uncontrolled), mechanical passive controller, and PID controller, respectively. By inspection of this figure, it can be seen that the values of the displacement x1 with PID controller is much less than with the passive controller.

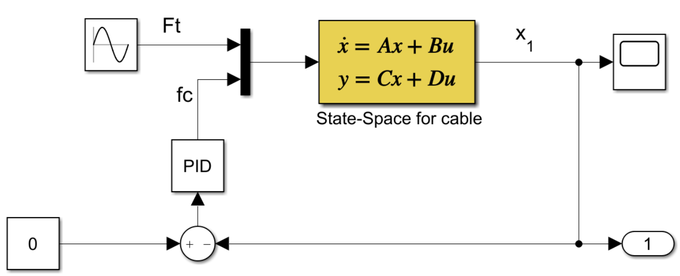

Fig.2 Simulation modelling for cable vibration control

The second control method is called 'Auto Tuneable Vibration controller'. The basic working principle is based on obtaining the stiffness, mass and damping coefficient in real time by tuning the control force *fc* , which is mathematically equivalent to the dynamic force of a passive vibration absorber. This control method was also verified by a series of simulation in MATLAB. Within same approach, displacement of cable x1 response is shown for with and without controller situations in time domain (see Fig.4). It is seen that, the obtained displacement result is gradually attenuated to the minimum value when compared with the free vibration case.

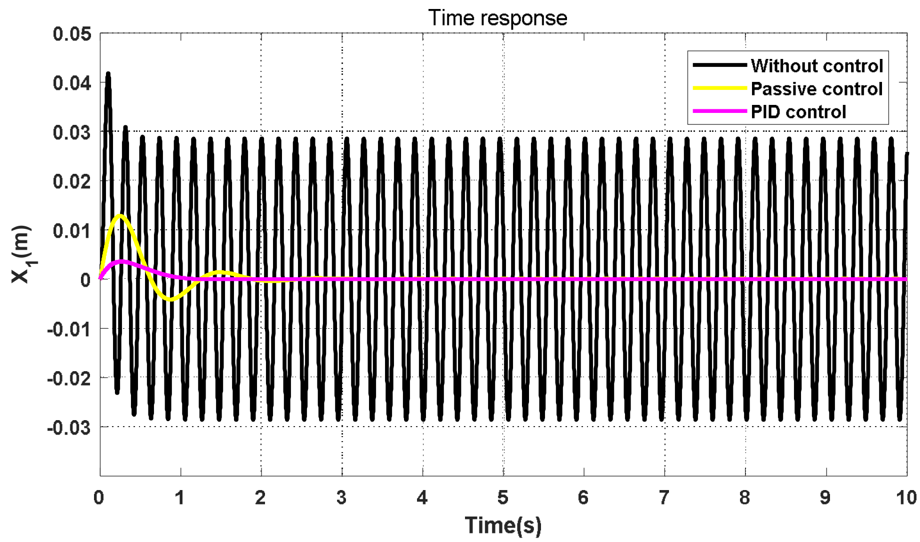

Fig.3 Time response result for using PID control

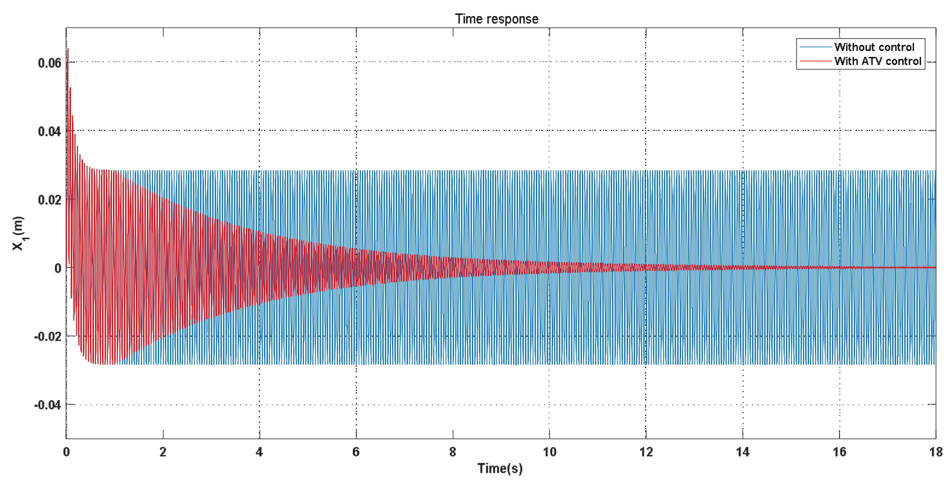

Fig.4 The displacement response of cable for using control and without using control

Conclusion

In this study, a simplified dynamic model of cable vibration was developed and implemented by using state-space model in MATLAB and SIMULINK. To control the vibration amplitude of the cable, PID control-based method was proposed and demonstrated a promising result compared with a mechanical passive controller. For the different industrial application, the second control methodology was also developed and implemented. The results indicate that the magnitude of vibration for different type of disturbance signal can be reduced in real time.

Acknowledgment

This paper was supported by the János Bolyai Research Scholarship of the Hungarian Academy of Sciences. The research was carried out in the frame of the project “EFOP-3.6.1-16-2016-00018 – Improving the role of research + development + innovation in the higher education

through institutional developments assisting intelligent specialization in Sopron and Szombathely”.

References

[1] Fujino, Y., K. Kimura, and H. Tanaka, *Wind resistant design of bridges in Japan: Developments and practices*. 2012: Springer Science & Business Media.

[2] Cigada, A., et al., *Vortex shedding and wake-induced vibrations in single and bundle cables.* Journal of Wind Engineering and Industrial Aerodynamics, 1997. **72**: p. 253-263.

[3] Barry, O., D.C. Oguamanam, and D.C. Lin, *Aeolian vibration of a single conductor with a Stockbridge damper.* Proceedings of the Institution of Mechanical Engineers, Part C: Journal of Mechanical Engineering Science, 2013. **227**(5): p. 935-945.

[4] Pipes, L.A., *Cable and damper vibration studies.* Electrical Engineering, 1936. **55**(10): p. 1149-1150.

[5] Wagner, H., et al., *Dynamics of Stockbridge dampers.* Journal of Sound and vibration, 1973. **30**(2): p. 207-IN2.

[6] Visioli, A., *Practical PID control*. 2006: Springer Science & Business Media.

[7] Ang, K.H., G. Chong, and Y. Li, *PID control system analysis, design, and technology.* IEEE transactions on control systems technology, 2005. **13**(4): p. 559-576.

Aerodynamic Performance Degradation due to Ice Accretion

Laszlo E. Kollár

Savaria Institute of Technology
ELTE Eötvös Loránd University, Budapest, Hungary
kl@inf.elte.hu

Abstract
Ice accretion on a 2D section of wind turbine blades is simulated with the specific aim to estimate the aerodynamic performance degradation of the iced blade. The ratio of the lift coefficient and the drag coefficient is calculated for the iced blade and compared with the same ratio obtained for the bare blade. This process is repeated for blade shapes with varying camber line, which provides the severity of aerodynamic performance degradation for different blade shapes.

Keywords: Aerodynamics, Icing, Simulation, Wind turbine

Introduction

Ice accretion on wind turbine blades worsens the aerodynamic performance of the wind turbine. Ice accretion reduces lift generation and increases drag, which leads to power loss of up to 50% at sites with high risk of icing [1]. These problems justify the research effort made to study numerically and experimentally the effects of icing on wind turbine blades. The main challenge in the design of wind turbine blades is to find the relationship between its shape and its aerodynamic properties. Garabedian & McFadden [2] developed an iterative procedure to design swept wings, which was later modified in [3] allowing design for a wide range of geometry with prescribed surface pressures. This procedure was applied in [4] where a correction factor was introduced in order to consider icing in the design process. The main goal is to determine aerodynamic performance degradation due to ice accretion on a set of blade shapes. The results will enable wind turbines to operate under a wide range of ambient conditions satisfactorily.

Methodology

Ice accretion on a set of shapes for wind turbine blades was simulated by applying a Matlab code, and then the aerodynamic coefficients were determined after the simulation of the air flow around the iced blade using Ansys Fluent. The set of blade shapes considered were determined by the NACA 4-digit airfoils with varying the first digit, i.e. NACA1412 to NACA8412. The first digit refers to the maximum camber of the airfoil, as shown in Fig. 1(a). Modelling icing consists of three main steps. First, the air flow field is modelled around the blade, then the motion of droplet trajectories is calculated in this air flow, and finally the ratio of frozen droplets is determined locally on the blade surface. The air flow around a bare blade is shown in Fig. 1(b). The present set of simulations assumed zero angle of attack. Once the iced shape is obtained, it is taken as input for Ansys Fluent that simulates the airflow around the iced shape and calculates the lift coefficient and the drag coefficient. The iced shapes as obtained after the Matlab computations and as introduced into Ansys Fluent can be seen in Fig. 2.

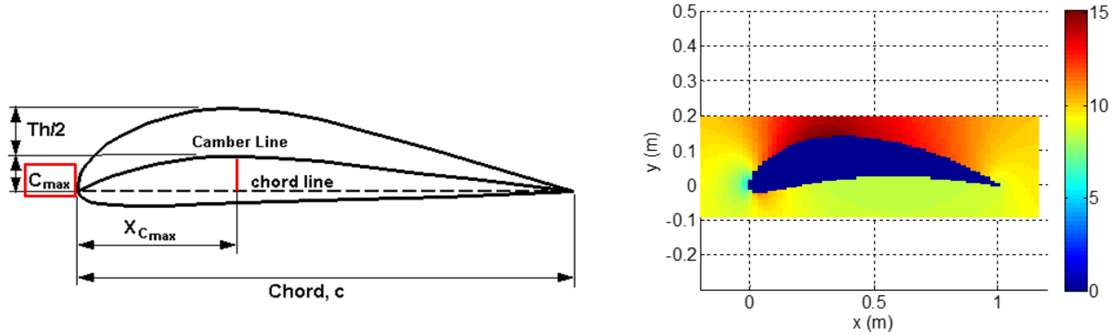

(a) (b)

Fig. 1: (a) Draft of a NACA 4-digit airfoil; (b) Air flow around the bare blade of NACA8412 shape

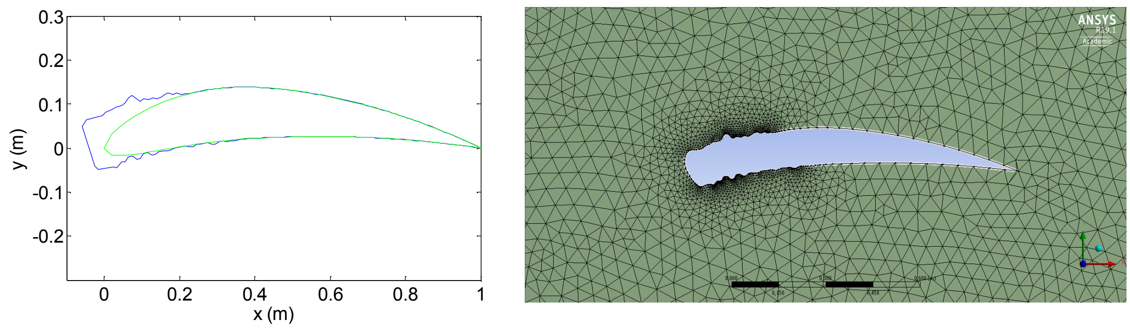

(a) (b)

Fig. 2: (a) Iced shape of the NACA8412 airfoil as obtained in Matlab computation; (b) Iced shape of the NACA8412 airfoil with mesh in Ansys Fluent

Parameters Influencing Aerodynamic Performance

The velocity distributions near the upper and the lower surfaces of the blade are defined by the performance criteria, and the corresponding blade shape is obtained after applying the inverse design process. Fig. 3 shows the velocity distribuitons around the NACA1412 and the NACA8412 airfoil shapes. The difference between velocities near the upper and lower surfaces at a given position along the chord length increases with the maximum camber. The parameter used to describe the aeroynamic performance of the blade is the lift-to-drag ratio. According to Table 1, this ratio increases with maximum camber until it reaches 5-6% of the chord length, and then it does not change significantly by further increasing the maximum camber.

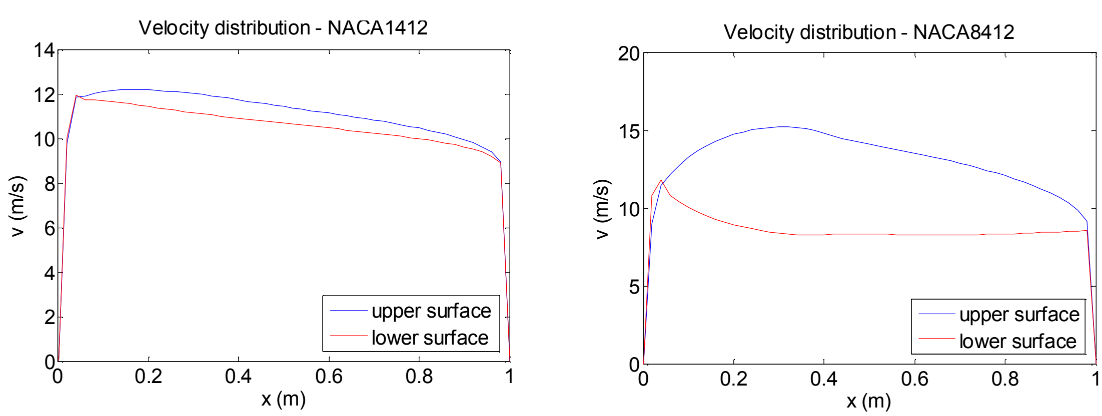

(a) (b)

Fig. 3: Velocity distributions near upper and lower blade surfaces (a) NACA1412 airfoil; (b) NACA8412 airfoil

Table 1: Aerodynamic coefficients of bare blades in NACA 4-digit airfoil shapes

velocity distribution	blade shape (airfoil)	lift coefficient C_L	drag coefficient C_D	lift-to-drag ratio C_L/C_D
1	NACA1412	0.108	0.0167	6.49
2	NACA2412	0.215	0.0171	12.55
3	NACA3412	0.329	0.0179	18.36
4	NACA4412	0.434	0.0191	22.74
5	NACA5412	0.533	0.0213	25.01
6	NACA6412	0.648	0.0221	29.32
7	NACA7412	0.760	0.0251	30.28
8	NACA8412	0.835	0.0286	29.20

Table 2: Lift-to-drag ratios for NACA 4-digit airfoil shapes (a) in-cloud icing; (b) freezing drizzle

Aerofoil	$(C_L/C_D)_{bare}$	$(C_L/C_D)_{iced}$	$\frac{(C_L/C_D)_{iced}}{(C_L/C_D)_{bare}}$
NACA1412	7.49	3.63	0.484
NACA2412	14.20	6.90	0.486
NACA3412	18.63	13.01	0.698
NACA4412	24.12	16.07	0.666
NACA5412	27.68	22.01	0.795
NACA6412	32.39	24.49	0.756
NACA7412	37.31	27.50	0.737
NACA8412	34.50	26.47	0.767

Aerofoil	$(C_L/C_D)_{bare}$	$(C_L/C_D)_{iced}$	$\frac{(C_L/C_D)_{iced}}{(C_L/C_D)_{bare}}$
NACA1412	6.49	0.77	0.119
NACA2412	12.55	1.53	0.122
NACA3412	18.36	4.25	0.232
NACA4412	22.74	6.70	0.294
NACA5412	25.01	8.63	0.345
NACA6412	29.32	9.11	0.311
NACA7412	30.28	13.86	0.458
NACA8412	29.20	13.34	0.457

Different icing conditions affects the aerodynamic performance to different extent. The aerodynamic coefficients were calculated for two substantially different icing conditions: in-cloud icing and freezing drizzle [5]. The lift-to-drag ratios for the bare and the iced blades are listed in Table 2 under these two conditions for different blade shapes. It can clearly be seen that the aerodynamic degradation is significantly more severe under freezing drizzle conditions than under in-cloud icing conditions.

Conclusions

Icing of wind turbine blades was simulated on a set of blade shapes under two different icing conditions, and aerodynamic performance degradation has been evaluated. The lift-to-drag ratio increases with maximum camber of the airfoil until it reaches 5-6% of the chord length, and then it does not change significantly by further increasing the maximum camber. Ice accretion on closely symmetric shapes (i.e. airfoil with small maximum camber) causes severe aerodynamic performance degradation; whereas it affects the aerodynamics of curved shapes to a lesser extent. The recommendation in regions with considerable risk of icing is to increase the maximum camber in the design process even if the required velocity distribution does not justify it. This recommendation would contribute to achive the goal that the wind turbine operates under some icing conditions.

Acknowledgment

This paper was supported by the János Bolyai Research Scholarship of the Hungarian Academy of Sciences. The research was carried out in the frame of the project "EFOP-3.6.1-16-2016-00018 – Improving the role of research + development + innovation in the higher education through institutional developments assisting intelligent specialization in Sopron and Szombathely".

References

[1] Parent, O., Ilnica, A., Anti-icing and de-icing techniques for wind turbines: Critical review, *Cold Reg. Sci. Technol.* 65, pp. 88-96, 2011.

[2] Garabedian P., McFadden, D., Design of supercritical swept wings, *AIAA Journal* 20, pp. 289-291, 1982.

[3] Malone, J.B., Vadyak J., Sankar L.N., Inverse aerodynamic design method for aircraft components, *J. Aircraft* 24, pp. 8-9, 1987.

[4] Kollár, L.E., Mishra, R., Inverse design of wind turbine blade sections for operation under icing conditions, *Energy Conversion and Management* 180, pp. 844-858, 2019.

[5] Kollár L.E., Farzaneh M., Modeling the evolution of droplet size distribution in two-phase flows, *Int. J. of Multiphase Flow* 33, pp. 1255–70, 2007.

The development of an intelligent vehicle control system.

Kristóf Lajber

Savaria Institute of Technology
ELTE Eötvös Loránd University, Budapest, Hungary
lk@inf.elte.hu

Abstract

The SZIe-Kart team has needed an easily expandable, robust, high performance control system for the Go-Kart Go-Bosch competition, which is capable to withstand the rough automotive environment. The system had to be flexible enough to solve the complex process control problems. Therefore I designed a modular system with microcontrollers, where the controllers are communicated trough CAN bus

Keywords: Intelligent driving, Self-driving, vehicle control system,

Introduction

I was part of a team at the student competition called Go-Kart Go-Bosch held by Bosch. The goal of the competition was to convert a traditional go-kart into a self-driving vehicle using components provided by Bosch. The components ware 12 Ultra Sound Sensors, a radar, a camera, several electric motors for the hybrid drive system(2 BLDC's), and for general purpose (2 DC), and a cordless drill for starter motor for the internal combustion engine. The other parts must be designed by the team. The vehicle should be able to do parallel, perpendicular parking with recognising the possible parking spot a home zone assist function, predictive braking, smart cruise control, and lane keeping functions. The milestones of the project can be seen on the following picture:

1. fig Milestones

Methodology

I have designed a modular control system based on Texas Instruments microcontrollers. In this system every major task got it's own microcontroller based control unit, for example the electric steering got its own module, where all the control logic happened, and the main control system only had to communicate the required steering angle to the module, but the main function does not required to include any logic regards how to reach that goal value.

Most of the required task needed some kind of input and / or feedback from the actuators. For this I had to choose proper sensors. I used a quite large range of sensors, from the most basic potentio meters to the 9 DOF MEMS sensor. The largest experience with these sensor ware, that the due the harsh environment the cheap "everyday use" sensors ware unreliable since they lack the sufficient environmental protection. To overcome this problem I choose industrial, and automotive grade components.

Ta achieve the required driver assistant functions I had to choose actuators too. For controlling the intake valve position on the carburettor of the petrol engine I choose a small servo unit. For the steering position I choose a second hand electric power steering from a car, and to manipulate the braking pedal position we used the wiper motor provided by Bosch.

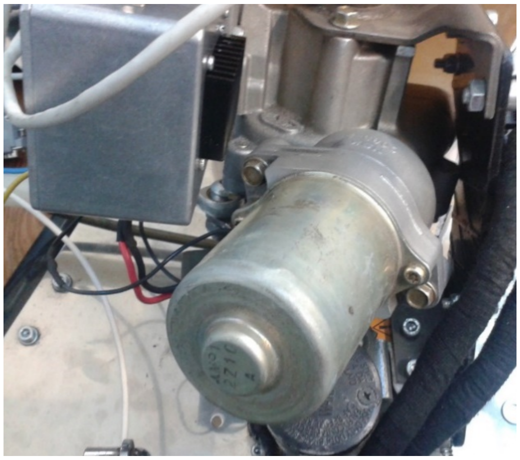

2. fig Power steering

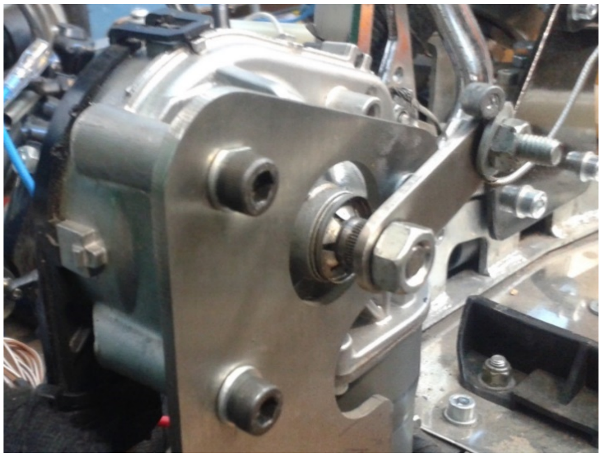

3. fig Wiper motor

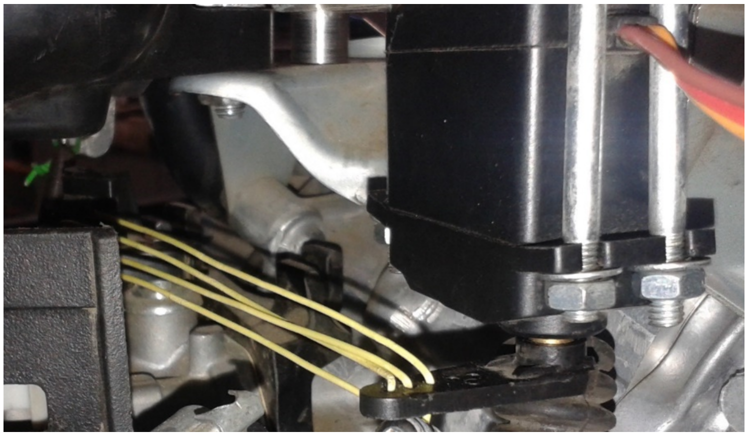

4. fig Servo unit

Results

The system proven itself during the competition, and made it possible to make it to the 3rd place in our category. The system could be used for further development since it has capacity for further development, and even after that it is quite easily expandable thanks to the CAN-bus communication.

Conclusions

The technical experience of the parcipating students ware significantly better after the project compared to the students, who did not take part in similar competitions. The main experience with the electronics that there is a huge gap between the “working on a table” and “working on a vehicle” electronics system. The control system has the potential for further development.

Acknowledgment

The project carried out in the frame of the Go-kart Go-Bosch competition.

The Designing of beam welding technologies for carbon steel structures

József Szőlősi

Savaria Institute of Technology
ELTE Eötvös Loránd University, Budapest, Hungary
szjo@inf.elte.hu

Abstract
This contribution describes the current production process of welding, as the research of technology can only stem from the awareness of the technological features and possibly of what waste could be eliminated in the original situation. The work is focusing on review the current research fields related to the topics of high-pressure welding, classical technology planning process and the conditions of weldability. Particularly, the production technology conditions of crack-free structures, with a special focus on defining the necessary pre-heating temperature, are discussed in detail. For the investigation I used the test results of the laserhybrid welding. These tests were performed with the professional support of welding technologies.

Keywords: welding technology, laser hybrid technology

Introduction

Since the 1950s, since welding science has opened up more and more professional perspectives, it is constantly changing. The reason for this is, of course, that the scientific results being integrated into professional everyday life have also resulted in significant progress in terms of economical efficiency for the individual companies.

The topic in the title of the dissertation today is of great actuality in the case of companies using several welding processes. Finding a reliable welding technology is a key issue in manufacturing technology, where economic issues are also of high importance. The essential part of the research is the development of a technology that can be used by industrial companies with appropriate cost efficiency.

In my dissertation, I am aiming to get to know more about advanced technologies, such as high-performance densities, and to identify problems associated with welding non-alloy industry-used structural steels.

Methodology

An important element of Technology Research was finding a reliable technology. *What is reliable technology in welding?*
Clearly, it means the production of crack-free production with adequate weldability. That is, the suitability of the steel complex for a given application, for a given process, with suitable welding materials, for a structure created with a given welding work order, in which the local properties of the metallic joints, together with their effect on the welded structure, meet the precise technical requirements. [1]. The following pictures illustrate the cases of failure during production in *Figure 1*.

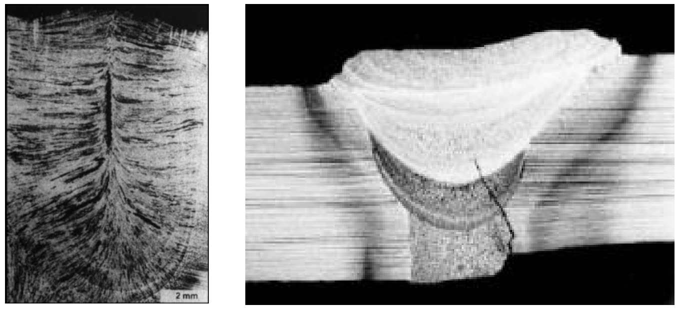

a.) b.)

Fig. 1: Failure cases a.) Hot-cracking [2]; b.) Typical example of root HAZ hydrogen crack extending into the weld metal [4]

For a crack-free work, calculations according to the MSZ EN 1011-2: 2001 *Welding. Recommendations for welding of metallic materials* standard series for preheating well known in welding technology are required. The Standards Collection has eight separate chapters. Apart from formulating the general guidelines, separate sections apply to the technology design guidelines for arc welding of ferrite steels, corrosion resistant steels, aluminium and alloys. In our case, the welding of ferritic steels is regulated by the standard MSZ EN 1011-2. According to the standard, the calculated pre-heating temperature of 100 ° C is required.

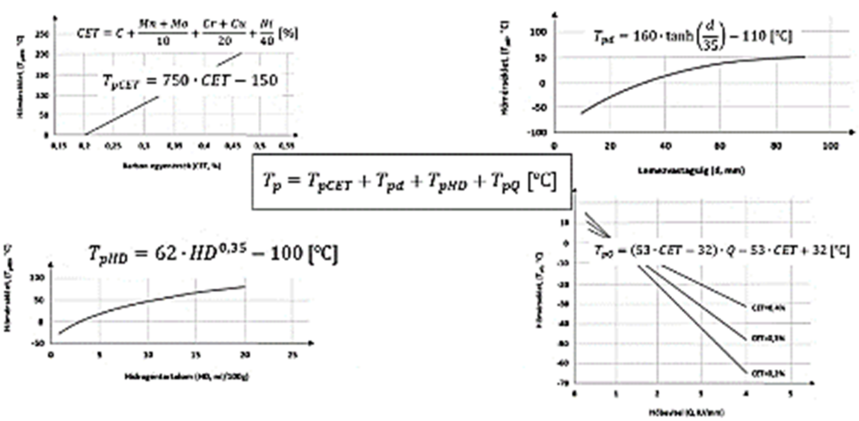

Fig. 2: Based on the calculations the preheating temperature

During the research, the aforementioned 10mm thick non-alloyed structural steel was welded by three methods, i.e., an open-loop (121-2), electron beam (51), laser beam (52) (laser hybrid) process. With the tests, I simulated welding cases with chamfer (nose height 5 mm) and without chamfer.

Welding was done with the following settings:

a.) Submerged arc welding: 1. wire: dia. 4.8mm; amperage: 1200A, volts: 32,5V; 2. wire: dia. 4.0mm; amperage: 500A, volts: 34V; welding speed: 110 cm/min; flux: EN ISO 14171 S A AB 1 57 AC H5

b.) Electron beam welding: EB generator volts: 60kV; welding speed: 15mm/sec; (without chamfering)

c.) Laser beam (laser hybrid) welding: TruDisk 6002 fiber laser; MIG: amperage: 219A, volts: 19,4V; welding speed: 80 cm/min;

Results

The tests were conducted according to the standard MSZ EN ISO 15614-1: 2004 *Specification and qualification of welding procedures for metallic materials. Welding procedure test* with special regard to hardness tests.

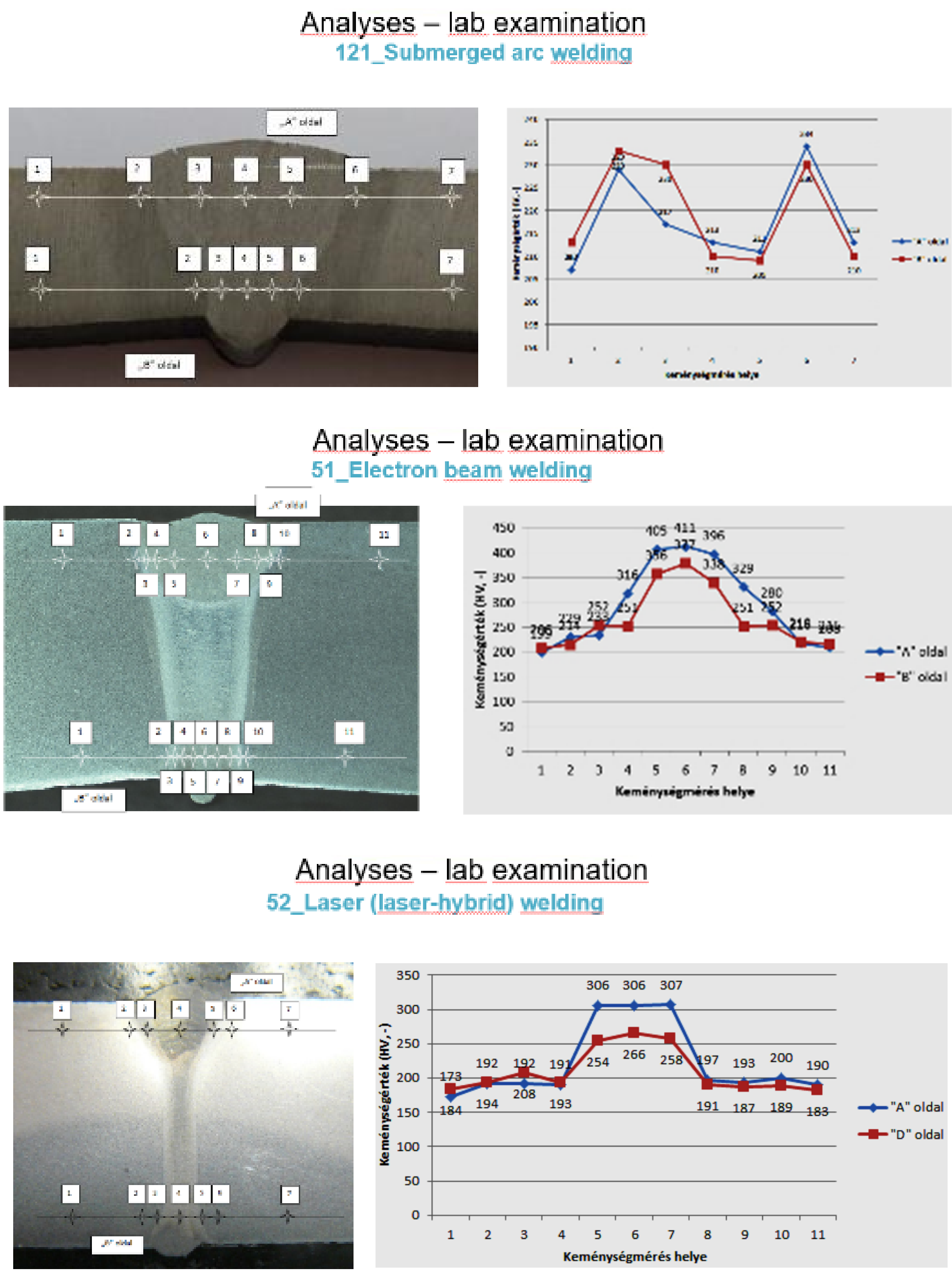

Fig. 3: Hardness tests during the lab examinations

Conclusions

At the end of the thesis, I evaluated the appropriateness of welding procedures according to the following criteria:

The form of the seam. Typically, the high-density procedures are characterized by a narrow seam. It has a less robust look compared to the submerged welding with high heat input. It is characterized by a narrow HAZ. The hardness, especially for electron beam welding, exceeds the hardness limit HV 380 as defined by the standard for welding technology in MSZ EN ISO 15614-1: 2004. *Specification and qualification of welding procedures for metallic materials. Welding procedure test.* The *Fig. 4.* shows the diagram with the hardness of each microstructure, which has a bainitic for submerged and the other, laser-beam welded structure and the martensitic structure in the case of electron beam welding. The hardness value of the cooling diagram in these areas is indicated by the hardness limit: in case of the laser beam not, but in the case of the electron beam-values it reaches it. According to the the hardness values only, it has to be said that the process carries the risk of failure of the welding due to the strain of the material structure.

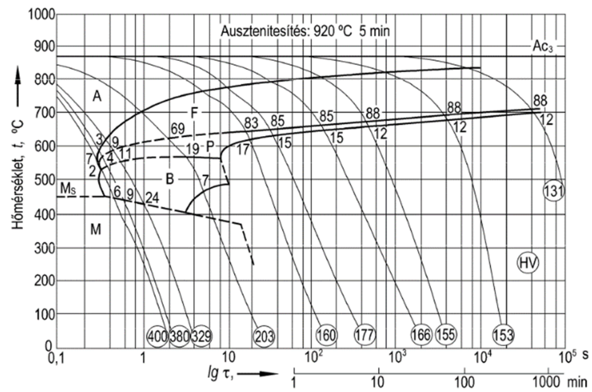

Fig. 4: Continuous austenitic transformation diagram for low carbon steel [3]

Crystallit size. There are many articles in the literature about the relationship between the fine grain structure and the flow limit mentioned in the paragraph. According to the Hall-Patch correlation, we can get an accurate picture of the strength by using the following equation shown in *Fig. 5.*

Accordingly, the increase in the crystallite size formed and the increase in the flow limit show an inverse proportionality. The degree of proportionality is clearly seen in the context below.

$$\sigma_y = \sigma_0 + k \cdot d^{-\frac{1}{2}} \qquad (1.)$$

where σ_y represents the lower flow limit, σ_0 represents the so-called friction stress (resistance to displacement movement to the crystal lattice), k is the constant (barrier parameter) for the material and d is the mean crystallit size.

Given the average particle size in both the heat-producing zones of both beam welding processes, the material has a flow limit (ReL) approaching 400MPa, which shows a similar strength to the base material.

Of course, in the development of technology, besides the adequacy of the production technology, the issues of being economical are also of great importance.

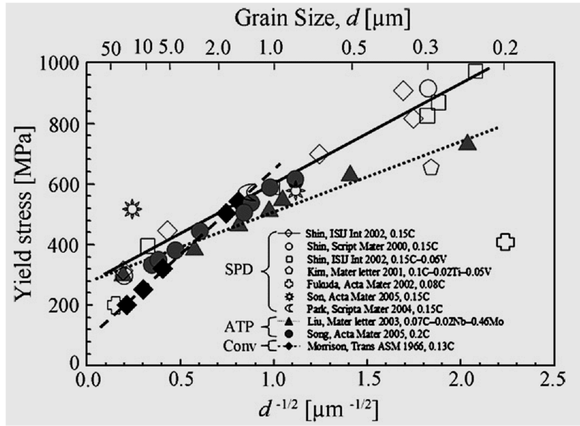

Fig. 5.: Hall-Petch correlation according to the results of R. Song and her colleagues [5]

Summary

As a background to my paper, I have described the current production process regarding welding, as the research of technology can only stem from the awareness of the technological features and possibly of what waste could be eliminated in the original situation. It was necessary to review the current research fields related to the theme, for which I used the national and international research reports and scientific journals of the topic. I reviewed the literature focusing on three main procedures and their subtypes.

References

[1] Szunyogh L (szerk.): Hegesztés és rokon technológiák. Budapest: Gépipari Tudományos Egyesület, Budapest, 2007.

[2] Komócsin Mihály: Anyagok hegeszthetősége. www.tankonyvtar.hu/hu/tartalom/tamop412A/2010-0013_anyagok_hegeszthetosege/4_2_szilardsagnovelo_mechanizmusok.html 2018.12

[2] Gáti József (szerk.): Hegesztési zsebkönyv, Cokom Mérnökiroda Kft., Miskolc, 2003.

[4] TWI Group: Technical Knowledge: *www.twi-global.com/technical-knowledge/published-papers/hydrogen-cracking-its-causes-costs-and-future-occurrence-march-1999/* 2018.12

[5] R. Song, D. Ponge, D. Raabe, J.G. Speer, D.K. Matlock: Overview of processing, microstructure and machenical properties of ultrafine grained bcc steels, Elsevier B.V., 2006.

Rolling mill design challenges

Tibor Borbély[2], Jurij J. Sidor

Savaria Institute of Technology
ELTE Eötvös Loránd University, Budapest, Hungary
bt@inf.elte.hu; js@inf.elte.hu

Abstract
In the laboratory-type investigations of the parameters of plastic forming technologies, significantly smaller equipment is used as compared to the industrial equivalents. The industrial rolling mills are generally suitable only for symmetrical rolling (the circumferential speeds of both cylinders are equal). The rolls for asymmetric rolling mill are driven by separate motors to achieve different circumferential speeds.
The work aims at the design of a laboratory rolling mill suitable for both symmetric and asymmetric rolling processes. In the project, it was necessary to implement the characteristics of the usual construction design, and also a specific feature of the device should be taken into account.
Using a rolling mill, which is suitable for asymmetric rolling, it is possible to ensure shear deformation in addition to compressive components. In conventional rolling, this scenario can be realized by cylinders of different roughness.

Keywords: Rolling mill, Symmetric rolling, Asymmetric rolling, Shear stress

Introduction

There are some solutions to get a laboratory-scale mill. The most expensive solution is to make a specialized design and and afterwards carry out the equipment. Cheaper solution is to purchase a new equipment, which is available on the market, or a used machine, but it usually does not meet all the requirements. It is possible to find local researchers who already developed similar mills, but generally they will not agree to sale their equipment. The next chance is to find a similar equipment, and convert it correspondingly. Another chance is own design and own production or production with an external firm. In the case of a university, usually there are no manufacturing capacity is available. In our case the best solution was the own design and manufacturing at the external firm.

Examination of existing constructions

The design process often starts with examining the existing constructions, because using the best solutions can significantly shorten the development time. We were given the opportunity to study semi-industrial and experimental rolling mill at the Laboratory of Materials Science at University of Miskolc. The experimental rolling mill developed and implemented by them can be seen in *Fig. 1*. It has been used as an example for the rolling mill designed by us.
The examined rolling mill has twin-engine drive and the cylinders are driven separately with two motors. The planetary drives of the motors and the cylinders are connected by classic spindles. The speed of the rollers can be varied independently of each other in the range of n=0-10 rpm. The table of the rolling mill has been specially developed because of the torque load on asymmetric rolling.

[2] Corresponding author

Fig. 1: Experimental rolling mill (University of Miskolc, Laboratory of Materials Science)

A larger rolling stand was constructed at the Laboratory of Materials Science as well. It is operated with the same twin planetary drives, as the first one (*Fig. 2*).

Fig. 2: The larger experimental rolling mill (University of Miskolc, Laboratory of Materials Science)

Development of a new construction

The designed rolling mill (as the sample rolling mill) has twin-engine drive with 2x7.5 kW power. The planetary drives of the motors and the cylinders are connected by Cardan shafts. The speed of the rollers can be varied independently of each other in the range of 0-10 rpm. The speed of the motors is changed by frequency inverters. The size of the rollers is ∅150x160 mm. The maximum rolling force is F_h=300 kN. The rolling torque was limited to T_h=1500 Nm by installing shear pins. The nominal torque of a Cardan shaft is T_C=5500 Nm. The table of the roll stand does not require any special foundation, because its design is so rigid that it does not have to be fixed to the base. The twin-engine drive and table are also suitable for driving a higher torque-driven roller stand, as the drive output torque is T_m=7000 Nm (at n=10 rpm). The 3D CAD model of the planned rolling mill is shown in *Fig. 3*.

The main parts of the rolling mill:
- Roller stand,
- Cardan shafts,
- Twin planetary drives,
- Table.

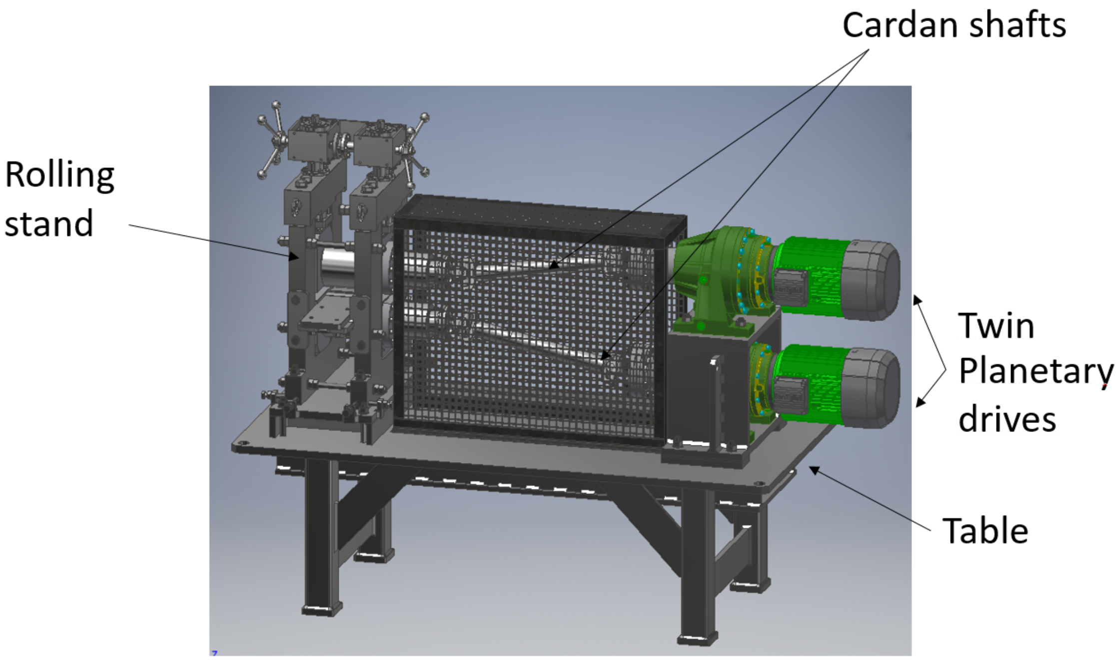

Fig. 3: CAD model of the rolling mill

The cylinders are made of hardened and tempered steel (X153CrMoV12), with self-aligning spherical roller bearing. The cylinder gap is adjustable between 0-25 mm with hand-driven worm-gear drives. (*Fig. 4-5*).

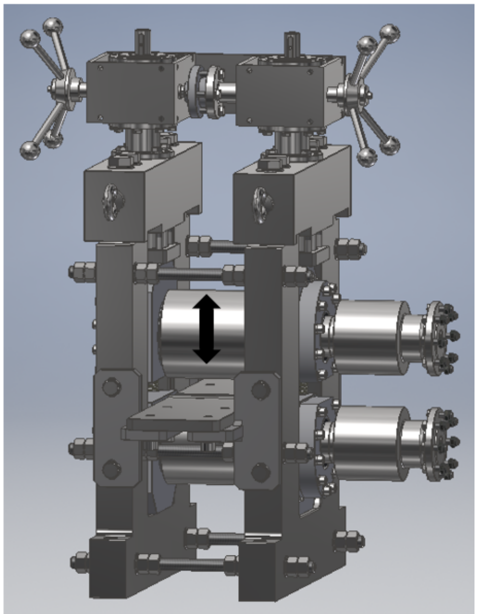
Fig. 4: CAD model of the rolling stand

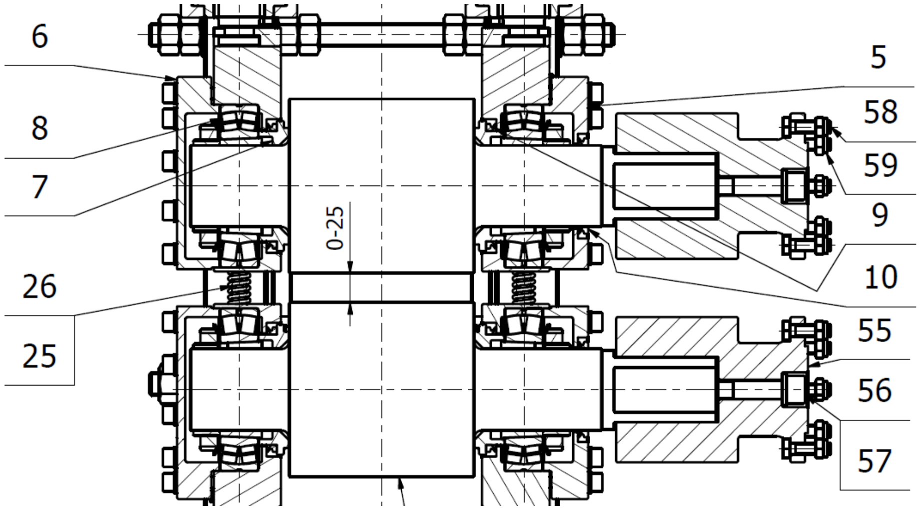

Fig. 5: Bearing of the roller cylinders

The main aim of designing the table of the rolling mill was to be able to absorb the rolling torque difference with minimal deformation during asymmetric rolling (*Fig. 6*).

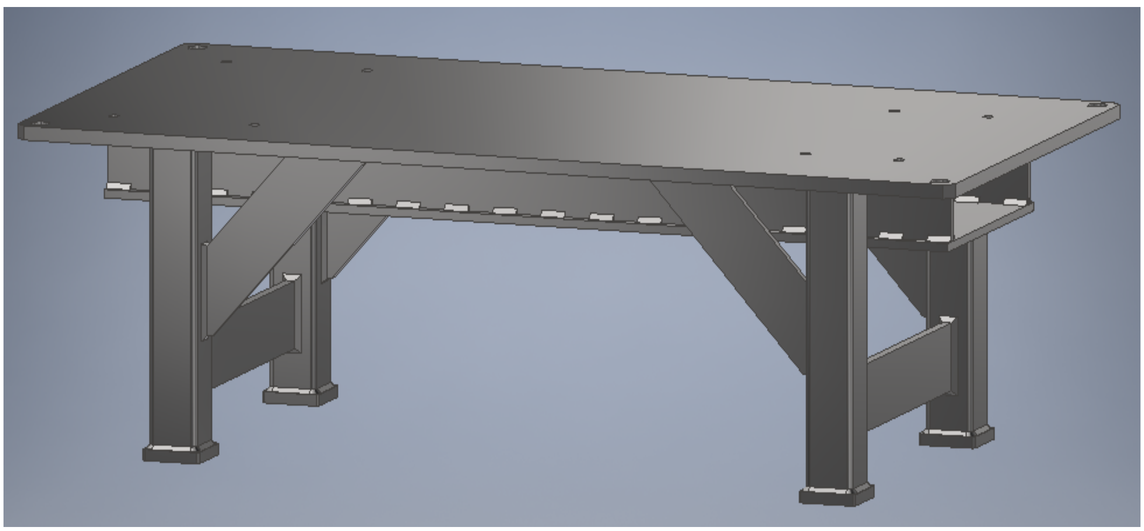
Fig. 6: Table

Conclusions

High shear-strain can be applied to the flat material during asymmetric rolling, resulting in significant strength increase. This requires separately variable circumferential speed cylinders. The planned rolling mill differs from the reference rolling mill in the following:
- motors and cylinders are conected with Cardan shafts instead of spindles,
- cylinders are fitted with rolling bearings instead of plain bearings, thus friction and wear is less,
- the upper cylinder can be moved with threaded spindles driven by synchronous worm gears, instead of hand-driven threaded spindles,
- the cabinet table does not require an attachment to the socket,
- the drive's chosen power and design of the table provide an opportunity to install a higher torque-driven roller stand.

Acknowledgment

The research was carried out in the frame of the project "EFOP-3.6.1-16-2016-00018 – Improving the role of research + development + innovation in the higher education through institutional developments assisting intelligent specialization in Sopron and Szombathely".

Finite Element Modelling of Deformation Flow in Symmetric and Asymmetric Rolling Processes

Daniel Fenyvesi[3], Jurij Sidor

Savaria Institute of Technology
ELTE Eötvös Loránd University, Budapest, Hungary
daniel.fenyvesi@inf.elte.hu; js@inf.elte.hu

Abstract
Processing technology of metals involves cold rolling, which triggers plastic deformation in a material, subjected to thickness reduction. In the course of symmetric rolling, the compressive component of the three-dimensional deformation tensor is dominating over other ones, whereas, the asymmetric mode accounts for a substantial amount of shear deformation. Additionally, the asymmetric loading is partially caused by both the different friction conditions of the surfaces and the variety in angular velocities of cylinders. This contribution discusses the results of finite element simulation (FEM) of 6063 aluminium alloy subjected to symmetric and asymmetric loading. Ansys Mechanical APDL solver was employed for the FEM calculations. The simulations were performed for non-linear static case, where the roll is considered as a rigid bogy, whereas the angular velocities of the upper and lower rolls were different with the aim to introduce asymmetry. In this two-dimensional calculation, it was assumed that the material rolled does not suffer any widening. It appeared that accurate simulation requires a high number of elements through thickness. Therefore, the number of elements across the thickness was varying between 10 and 12. Results of the FEM simulations are presented in a form of strain velocity gradients, strain and stress distributions across the thickness of rolled sheets.

Keywords: FEM simulation, cold rolling, aluminium sheets

Introduction

Plastic anisotropy of rolled materials is attributed to the development of crystallographic texture. In Al alloys, which are used in automotive industry, the poor formability is caused by specific texture, which tend to evolve during both rolling and subsequent recrystallization.

The process of formability involves a wide spectrum of deformation modes, whereas the process is mainly controlled the work-hardening coefficient, the strain rate sensitivity and the normal anisotropy [1]. The last parameter is closely related to the texture.

The main goal of this work is to analyse the effect of technological parameters on the strain mode, which conditions the evolution of texture [1]. the deformation gradients and strain velocity gradients of rolled sheets were calculated by means of finite element model. The components of strain velocity tensor will be used us as an input parameters for crystal plasticity calculations.

Methodology

The FEM model is nonlinear static because the sample suffer from inelastic deformation. Therefore, the material model is Bilinear Isotropic Hardening (BIH) [2]. The properties of the applied material shown in Table 1.

[3] Corresponding author

Table 1. The properties of aluminum material (Al6063)		
Density	2690	[kg/m^3]
Young's modulus	68300	[MPa]
Poisson's ratio	0.33	
Bulk modulus	$6.6961 \cdot 10^{10}$	[Pa]
Shear modulus	$2.5677 \cdot 10^{10}$	[Pa]
Tensile stress at Yield	176	[MPa]
BIH tangent modulus	441	[MPa]

Tensile diagram of the Al 6063 edited from the Table 1. shown in Fig. 1.

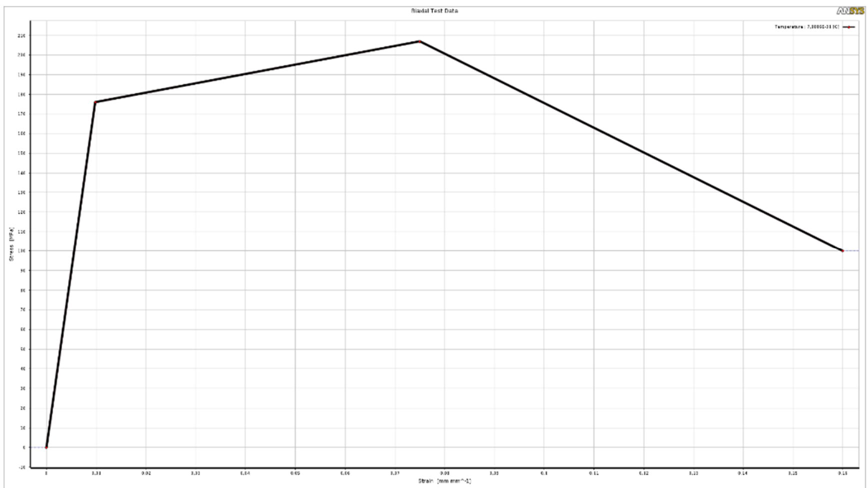

Fig. 1. Tensile diagram of the Al 6063

Because transverse deformation is negligible, the model is 2D. The sample and work-rolls 2D CAD model and boundary conditions shown in Fig. 2.

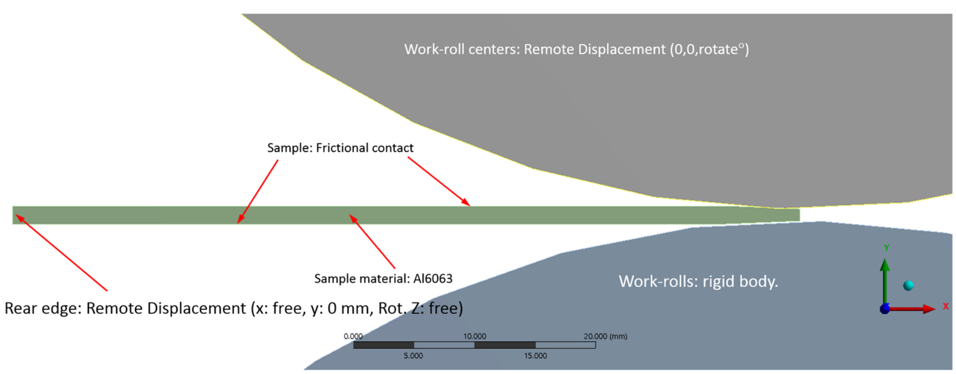

Fig. 2. The 2D CAD model and boundary condition

The Coulomb coefficient of friction is assumed to be 0.1. Discretization of geometry was done with quadrilateral mesh (Fig. 3.). The number of elements across the thickness was set to 10.

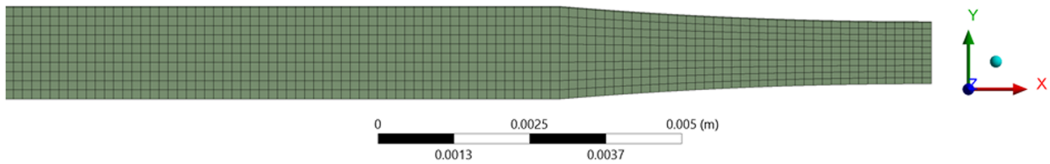

Fig. 3. The sample was discretized quadrilateral mesh

The asymmetry of the load is caused by the different angular speed of the work-rollers:

- Symmetric case, $\omega_{upper} = \omega_{lower} = 3$ [rad/s].
- Asymmetric case, $\omega_{upper} = 2$ [rad/s], $\omega_{lower} = 3$ [rad/s].

Definition of deformation gradient and strain velocity

In our calculation two vectors characterize the edges of the quadrilateral cell [3] (Fig. 4.).

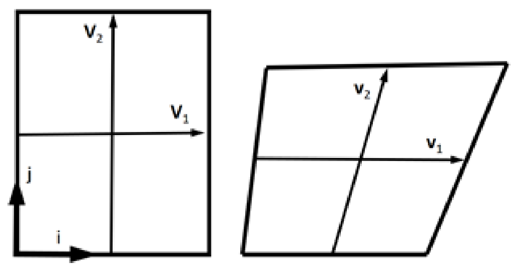

Fig. 4. Quadrilateral element before (left) and after deformation.

Prior to deformation, the vectors link the middle of the opposite sides of a given square (Fig. 4.).

$$\mathbf{V}_1 = \mathrm{A}\mathbf{i} + \mathrm{B}\mathbf{j}$$
$$\mathbf{V}_2 = \mathrm{C}\mathbf{i} + \mathrm{D}\mathbf{j} \qquad (1)$$

After rolling, the vectors are [3]:

$$\mathbf{v}_1 = \mathbf{a}\mathbf{i} + \mathrm{b}\mathbf{j}$$
$$\mathbf{v}_2 = \mathbf{c}\mathbf{i} + \mathrm{d}\mathbf{j} \qquad (2)$$

The calculation of the deformation gradient tensor **F** was performed at the centroid of each element according to procedure, described in ref. [3]:

$$\begin{bmatrix} a & c \\ b & d \end{bmatrix} = \boldsymbol{F} \begin{bmatrix} A & C \\ B & D \end{bmatrix} \Rightarrow \boldsymbol{F} = \begin{bmatrix} a & c \\ b & d \end{bmatrix} \begin{bmatrix} A & C \\ B & D \end{bmatrix}^{-1} \qquad (3)$$

Consequently, the strain velocity can be calculated as:

$$L = \dot{F} \cdot F^{-1} \approx \frac{\Delta F}{\Delta t} F^{-1} \tag{4}$$

Results

The equivalent stress distribution

➢ Symmetric case.

As Fig. 5 shows, the deformation from the surface towards the centre is developed immediately after the material enters the roll gap.

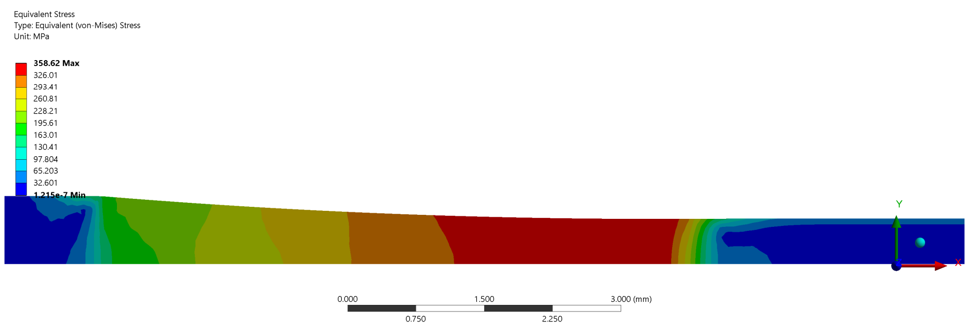

Fig. 5. Equivalent stress distribution in the symmetric case.

➢ Asymmetric case (Fig. 6.).

As Fig. 6 reveals, the peak stress domain extends towards the lower/slower work-roll. The peak value of the equivalent stress is not affected by the asymmetry.

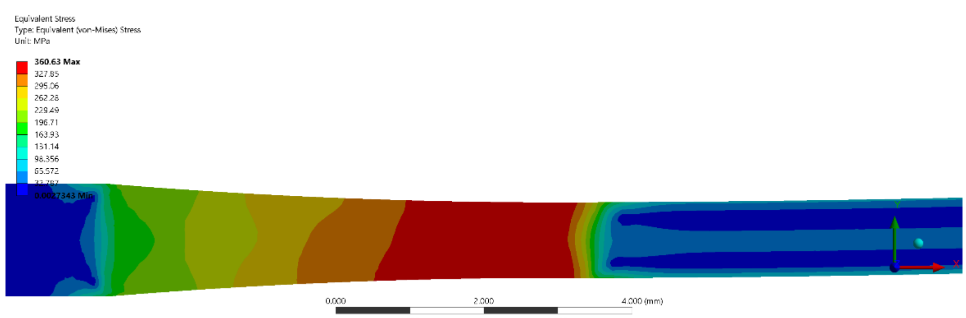

Fig. 6. Equivalent stress distribution in the asymmetric case.

The maximum principal stresses

In both cases (Fig. 7. and Fig. 8.) the peak values converges into a point at the surface at the entrance and exit of the deformation zone. The peak values are the same in both cases.

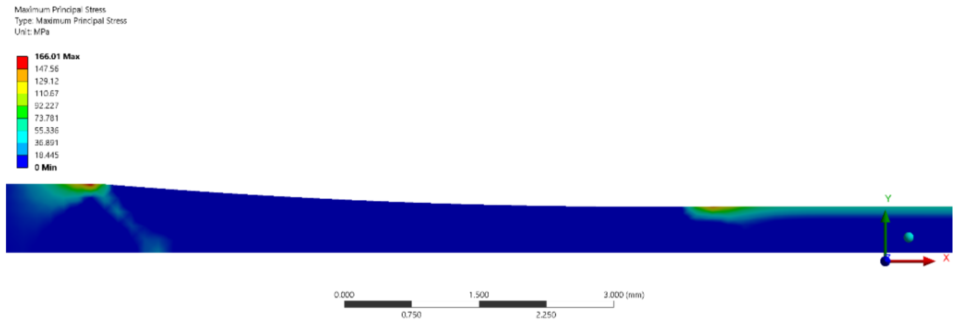

Fig. 7. The maximum principal stresses in the symmetric case.

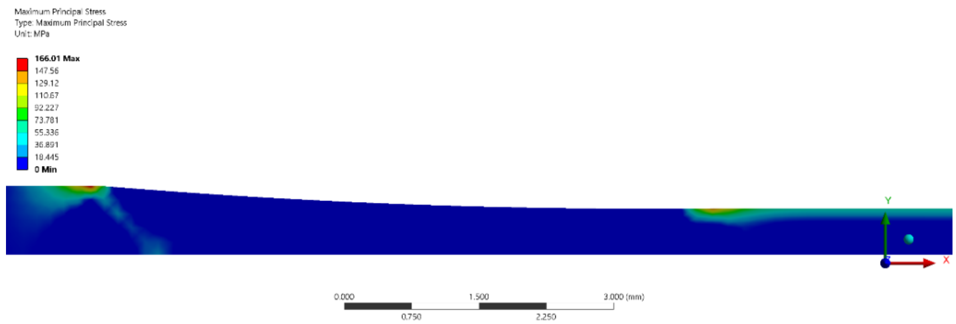

Fig. 8. The maximum principal stresses in the asymmetric case.

Example of calculated strain velocity gradient

➢ Symmetric case (5th cell, Fig. 9. and Fig. 10.).

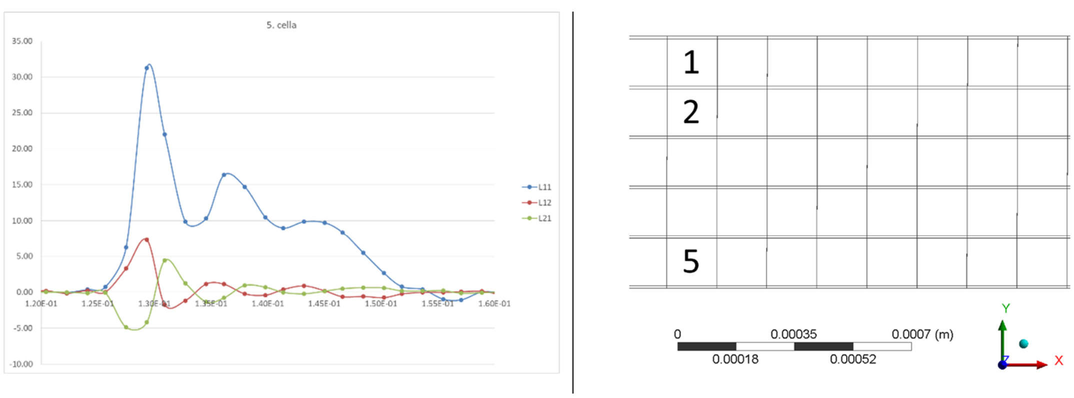

Fig. 9. Calculated strain velocity gradient in the symmetric case.

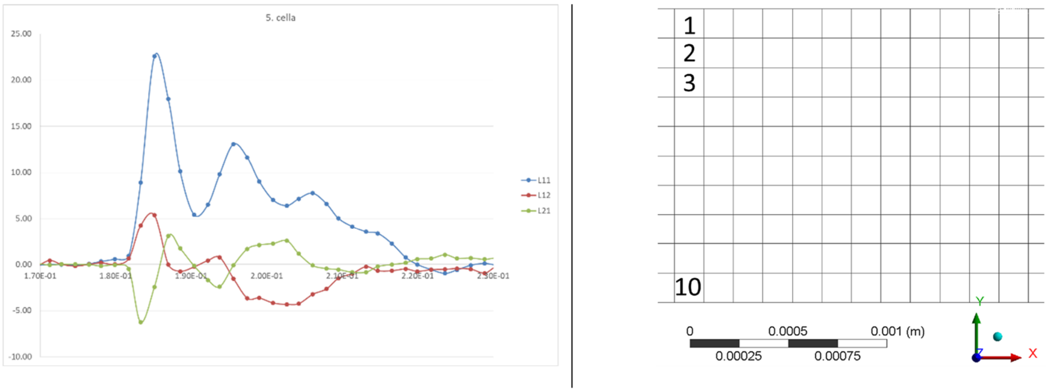

Fig. 10. Calculated strain velocity gradient in the asymmetric case.

Conclusions

Both strain gradients and strain velocity gradients can be successfully calculated by the proposed method.

Results of our calculations show that strong strain gradient evolves across the thickness of a rolled sheet. This is more pronounced in the case of asymmetric rolling.

Results of the FEM simulations should be calibrated by means of comparison between the experimental and calculated counterparts.

Acknowledgment

The research was carried out in the frame of the project “EFOP-3.6.1-16-2016-00018 – Improving the role of research + development + innovation in the higher education through institutional developments assisting intelligent specialization in Sopron and Szombathely”.

References

[1] Sidor J. et al., *Microstructural and crystallographic aspects of conventional and asymmetric rolling processes,* Acta Materialia, v56, pp. 2495-2507, 2008.

[2] Ansys mechanical APDL material reference, ANSYS, 2015.

[3] Boldetti, C. et al., *Measurement of deformation gradients in hot rolling of AA3004, Experimental mechanics*, v45, No. 6, 2005.

Brief Review on Comparison of Microstructure Evolution during Symmetric and Asymmetric Rolling

Gyula Pál[4], Jurij J. Sidor

Savaria Institute of Technology
ELTE Eötvös Loránd University, Budapest, Hungary
gp@inf.elte.hu, js@inf.elte.hu

Abstract
The microstructure and crystallographic texture of a metal sheets has a strong relationship with the anisotropy of properties. The present study aims to examine the relation between the mechanical behaviour and different processing methods.
Keywords: Aluminium, Anisotropy, Symmetric rolling, Asymmetric rolling, Microstructure

Introduction

Aluminium is a widely used material in the automotive industry due to its prosperous characteristics. Its density of 2,71 g/cm^3 (approximately 3x lighter than steel) and good corrosion resistance makes it a popular substitute of the structural steel. But these favourable properties are accompanied with some drawbacks, such as the poor deep-drawability (compared to steel). The following defects might occur during the deep-drawing: cracking, surface quality deterioration, earing and so on.
These problems have been practically avoided by using of exaggerated material thickness by the manufacturing technologists based on empirical factors. This solving method is regularly leading to excessive material usage, which could be saved by a more sophisticated method.
If we load a sample during a tensile test with a force and measure the true strains, we can calculate the Lankford value (also called normal anisotropy) by the following formula:

$$r = \frac{\lambda_b}{\lambda_s} = \frac{ln\frac{b}{b_0}}{ln\frac{s}{s_0}} \tag{1}$$

where: λ_b = real elongation in the direction of width
λ_s = real elongation in the direction of thickness

For the good deep-drawing characteristics it is important, that during the process in the direction of thickness the dimensional change should be lower, than in the direction of width. Based on the previous correlation the deep drawability of an inspected material can be considered good, if the $r > 1$ [1].
The normal anisotropy of a rolled sheet depends on the direction. Because of this, we also should measure the elongation in different directions with respect to rolling direction (RD). Generally, these angles are: 0°, 45° and 90° (see Fig. 1).

[4] Corresponding author

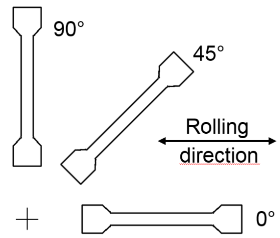

Fig. 1. Specimens cut out from a rolled sheet

With the cut-out samples based on Fig. 1 we can calculate the average Lankford value, which is calculated by the following formula [3]:

$$\bar{r} = \frac{r_0 + r_{90} + 2 \cdot r_{45}}{4} \tag{2}$$

The desired value for reasonable deep-drawability is $\bar{r} > 1.1$ [1].
If the average r exceeds the value of 1, the wall cracking could be avoided. To avoid the phenomenon of earing we should consider the planar anisotropy Δr which can be calculated by the formula:

$$\Delta r = \frac{1}{2} \cdot (r_0 + r_{90} - 2 \cdot r_{45}) \tag{3}$$

In ideal case, the normal anisotropy supposed to be equal to zero.
The anisotropy is crystallographic texture related, and in order to effect it, it is necessary to produce a material with corresponding texture, while other microstructural parameters such as grain size should remain under control.

Discussion

As it is concluded in Refs. [2-3], the evolution of crystallographic texture in Al alloys occurs according to the scheme, presented in Fig.2, while microstructure refinement can be achieved by asymmetric rolling.

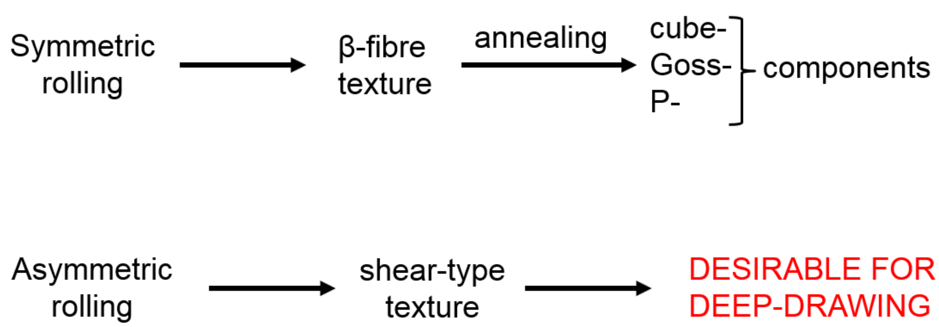

Fig.2. Schematic representation of texture evolution in symmetric and asymmetric rolling.

Conclusions

The following conclusion can be made based on literature review:

1. The deep-drawability of Al alloys can be improved by texture modification.

2. Asymmetric rolling tends to enhance the shear-type texture components, while the conventional rolling leads to the evolution of so-called β-fibre.

3. During recrystallization, the β-fibre transforms to the cube-Goss and P orientations, which account for strong planar anisotropy and therefore, poor drawability. In contrast, the asymmetrically rolled materials reveal a new-type of texture, which ensure improved deep-drawing characteristics.

Acknowledgment

The research was carried out in the frame of the project "EFOP-3.6.1-16-2016-00018 – Improving the role of research + development + innovation in the higher education through institutional developments assisting intelligent specialization in Sopron and Szombathely".

References

[1] László Horváth, *Mélyhúzás lemezanyagai és minősítési módszereik*. Óbuda University, Donát Bánki Faculty of Mechanical and Safety Engineering, 2009

[2] Jurij Sidor, Alexis Miroux, Roumen Petrov, Leo Kestens, Microstructural and crystallographic aspects of conventional and asymmetric rolling processes, Acta Materialia 56 (2008) 2495–2507

[3] Jurij Sidor, Roumen H. Petrov, Leo A.I. Kestens, Deformation, recrystallization and plastic anisotropy of asymmetrically rolled aluminum sheets, Materials Science and Engineering A 528 (2010) 413–424

Application of polycrystal models to simulation of texture evolution in thermo-mechanical processing of metals

Jurij J. Sidor

Savaria Institute of Technology
ELTE Eötvös Loránd University, Budapest, Hungary
js@inf.elte.hu

Abstract
The evolution of crystallographic texture in a polycrystalline aggregate, subjected to thermomechanical processing, tends to induce a strong anisotropy of properties. The processing parameters strongly affects the mesoscopic transformations in metals, however, the influence of a particular technological parameter is not always unambiguous. In this view, implementation of reliable computational approach is of crucial importance. Current contribution focuses on the implementation of various models in prediction of texture evolution in Al alloys during processing. Based on crystal plasticity simulations conducted, it can be revealed how model parameters affect the quality of texture prediction.

Keywords: Al alloys, crystal plasticity, texture, modelling

Introduction

Industrially produced metals are usually polycrystalline aggregates with characteristic crystallographic textures. The key microstructural feature such as a grain size is strongly correlated to mechanical properties, however, the anisotropy of properties is mainly affected by means of texture evolved. The evolution of texture occurs over the entire thermo-mechanical processing and the control of this development occurs via tuning of manufacturing parameters. The degree of reduction, number of deformation steps, annealing temperature or heating/cooling rate have a strong impact on both microstructure and texture development. In this view, it is very important to control the key microstructural parameters during each production step and this is possible via linking the external macroscopic influences to the mesoscopic features. The numerical approaches are of great importance in resolving this issue. The aim of the current contribution is to employ various polycrystal models in prediction of texture evolution.

Methodology

AA 6016 aluminum alloy was investigated in the current study. The alloy was heat treated at 550°C prior to rolling. The annealed material (1.125 mm thick) was cold rolled to a final with 18% reduction in one pass.
The through-thickness textures before and after cold rolling were measured by electron backscattering diffraction (EBSD) detector attached to the scanning electron microscope (SEM) FEI®. The orientation contrast scans were collected and analysed by the commercial OIM-TSL-7® software. The acceleration voltage of SEM was kept in the range of 15-20kV. During the EBSD measurements, the investigated samples were 70° tilted with respect to the detector. The OIM data were acquired on a hexagonal scan grid. The EBSD measurements were carried out in the plane perpendicular to the sample transverse direction covering the entire thickness of the investigated sample.

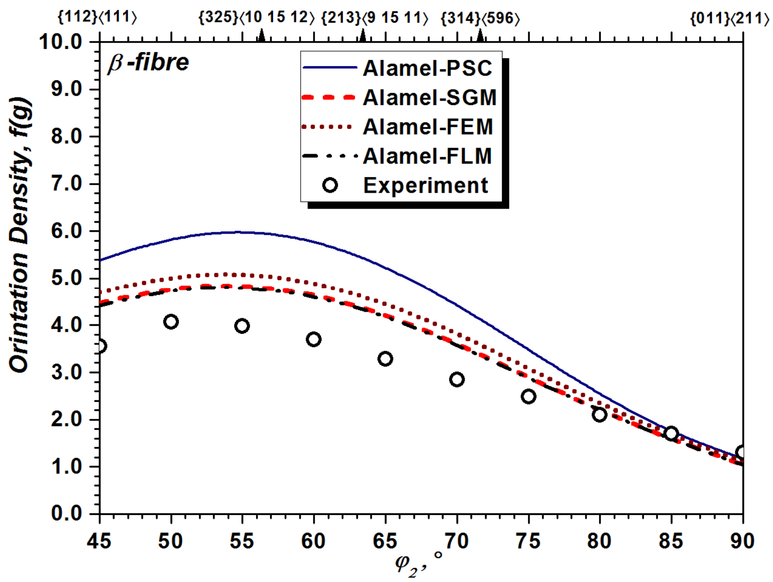

Fig. 1: Distribution of orientation intensities along the β–fibre. In the crystal plasticity calculations performed by the Alamel model the strain mode was approximated by various models: PSC, SGM, FLM and FEM.

The texture evolution during cold rolling was predicted by taking into account the {111}<110> octahedral slip systems. The advanced lamel (Alamel) model [1, 2] was employed for crystal plasticity calculations.

The strain velocity gradient tensors were calculated for the crystal plasticity models employed. The rolling was approximated by plane strain compression, however this approach disregards heterogeneous nature of strain distribution, therefore, in order to ensure more accurate approximation of displacement fields through the thickness, more sophisticated approaches were involved. Finite element computations (FEM), flow-line modelling (FLM) [3] and calculations by the so-called simple geometric model (SGM) [4] were performed for more accurate texture simulation. In the FEM, material's hardening was described with the stress-strain curve, while in the SGM and FLM the strain hardening effect was neglected.

Results, obtained by combining crystal plasticity with corresponding continuum mechanics-based approach, i.e. PSC-Alamel, FEM- Alamel, FLM- Alamel, and SGM- Alamel, were compared with the experimentally measured texture.

Results and discussion

In materials with FCC crystal structure, the initial texture tends to rotate towards the β-fiber described analytically by the following equation [5]:

$$\{h, \quad 1, \quad h+1\}\left\langle \frac{h(h+1)}{3/4-h}, \quad \frac{2h(h+1)}{1/2-h}, \quad \frac{h^2}{h-3/4}+\frac{2h}{h-1/2} \right\rangle \qquad (1)$$

The evolution of texture after 18% thickness reduction in the investigated Al alloy is presented in Fig.1. As Fig.1 shows, the intensity along the β-fiber tends to decline while moving from the Copper $\{112\}\langle 111\rangle$ towards the Brass $\{101\}\langle 121\rangle$ component. This trend is accurately captured by the CP approach employed. This crystal plasticity theory accounts for short-range grain interaction phenomena during deformation. It is obvious (see Fig.1) that disregarding strain heterogeneity across the thickness (PSC mode) lead to significant discrepancies between the computed and experimentally measured texture intensities. The accuracy of texture simulations has significantly improved when the strain mode was calculated by the approaches, which take into account the heterogeneous nature of shear strain distribution (FEM, FLM and SGM) across the thickness of a rolled material.

Conclusions

Results of crystal plasticity simulations suggest that employing models, which are capable of considering the strain heterogeneity through the thickness of a rolled sheet, accounts for an improvement in the quality of texture simulations. It turned out that analytical approaches such as simple geometric model as well as flow line model tend to produce a result similar to one predicted by the FEM.

Acknowledgment

This work was carried out in the frame of the project "EFOP-3.6.1-16-2016-00018 – Improving the role of research + development + innovation in the higher education through institutional developments assisting intelligent specialization in Sopron and Szombathely".

References

[1] Van Houtte P, Li S, Seefeldt M, Delannay L, Deformation texture prediction: from the Taylor model to the advanced Lamel model *Int. J. Plast.* **21,** 2005, 589-624.

[2] Van Houtte P, Kanjarla A K, Van Bael A, Seefeldt M, Delannay L, Multiscale modeling of the plastic anisotropy and deformation texture of polycrystalline materials *European J. Mech. A/Solids,* **25,** 2006, 634-48.

[3] Decroos K, Sidor J, Seefeldt M, A new analytical approach for the velocity field in rolling processes and its application in through-thickness texture prediction *Met. Mater. Trans. A,* **45,** 2014, 948-961.

[4] Sidor J. J, Deformation texture simulation in Al alloys: continuum mechanics and crystal plasticity aspects *Model. Sim. Mater. Sc. Eng.,* ***26***, 2018**,** 085011.

[5] Sidor J J, Kestens L. A. I, Analytical description of rolling textures in face-centred-cubic metals *Scripta Mater.* **68,** 2013, 273-76.